Climate Dynamics (2001) 18: 29–49

K. Ide · H. Le Treut · Z.-X. Li · M. Ghil

Atmospheric radiative equilibria. Part II: bimodal solutions for atmospheric optical properties

Received: 7 December 1999 / Accepted: 19 February 2001

Abstract A simple theoretical model of atmospheric radiative equilibrium is solved analytically to help understand the energetics of maintaining Earth's tropical and subtropical climate. The model climate is constrained by energy balance between shortwave (SW) and longwave (LW) radiative fluxes. Given a complete set of SW and LW optical properties in each atmospheric layer, the model yields a unique equilibrium-temperature profile. In contrast, if the atmospheric temperature profile and SW properties are prescribed, the model yields essentially two distinct LW transmissivity profiles. This bimodality is due to a nonlinear competition between the ascending and descending energy fluxes, as well as to their local conversion to sensible heat in the atmosphere. Idealized slab models that are often used to describe the greenhouse effect are shown to be a special case of our model when this nonlinearity is suppressed. In this special case, only one solution for LW transmissivity is possible. Our model's bimodality in LW transmissivity for given SW fluxes and temperature profile may help explain certain features of Earth's climate: at low latitudes the temperature profiles are fairly homogeneous, while the humidity profiles exhibit a bimodal distribution; one mode is associated with regions of moist-and-ascending, the other with dry-and-subsiding air. The model's analytical results show good agreement with the European Centre for Medium-Range Weather Forecasts' reanalysis data. Sensitivity analysis of the temperature profile with respect to LW transmissivity changes leads to an assessment of the low-latitude climate's sensitivity to the "runaway greenhouse" effect.

K. Ide · M. Ghil
Department of Atmospheric Sciences and Institute of Geophysics and Planetary Physics, University of California, Los Angeles, California 90095-1565, USA

H. Le Treut (✉) · Z.-X. Li
Laboratoire de Météorologie Dynamique du CNRS, Université P. et M. Curie, case courrier 99, Tour 25, 5e etage 4 place Jussieu, 75252 Paris Cedex 05, France
E-mail: Herve.Letreut@lmd.jussieu.fr

1 Introduction and motivation

1.1 Idealized representation of the tropical climate

Idealized single-column models have been widely used by the climate community as a tool to investigate a variety of radiative-convective phenomena in the atmosphere and oceans. Fundamental knowledge gained by studying such models can deepen our understanding of climate processes as well as help us develop more sophisticated models to simulate them. Recent applications of such single-column models to low-latitude atmospheric physics include: (1) climate stability enhancement due to the "thermostat hypothesis" of Ramanathan and Collins (1991, 1993) and subsequent investigations (e.g., Fu et al. 1992, 1996; Lau et al. 1994; Pierrehumbert 1995, who used a two-box model; Bony et al. 1997, and references therein); and (2) multiple equilibria (Li et al. 1997; Rennó 1997) and oscillations (Hu and Randall 1994) in the Earth's atmosphere.

Observations of the tropical atmosphere on different time scales raise fundamental questions about the mechanisms that maintain radiative-convective equilibrium or act to modify it. For example, paleoclimatic records of sea-surface temperature in the tropics indicate that Earth's tropical climate was fairly stable on the time scale of millenia (CLIMAP 1976, 1984).

On intraseasonal time scales, on the other hand, the Madden-Julian (1971) oscillation involves substantial variability in both dynamical and thermodynamical fields. It is characterized by eastward-propagating Kelvin waves that interact with (Emanuel et al. 1994; Neelin and Yu 1994) or may be due entirely to (Hu and Randall 1994) instabilities of radiative-convective equilibrium.

Simple column models are generally all based on solving for the balance of radiative and nonradiative

energy fluxes, possibly subject to distinct boundary conditions such as land-surface fluxes or ocean forcing. In order to investigate the nature and stability of the vertical temperature-and-humidity profiles in the low-latitude climate system, numerous hypotheses have been formulated, depending on the focus of each study. Some of these hypotheses, however, may seem to contradict each other.

Ramanathan and Collins (1993) relied on the *homogeneous* description of the entire tropical atmosphere as a single convective column in their thermostat-hypothesis work. This homogeneity is consistent with certain dynamical constraints, such as conservation of angular momentum, that require the temperature profile to be homogeneous throughout the tropical belt (Peixoto and Oort 1992; James 1994, and references therein). The observations indeed show that the atmosphere has a homogeneous distribution of the vertical temperature profile throughout the tropics, whether it be in a moist or dry region (Peixoto and Oort 1992; see also our discussion in Sect. 3.1).

Pierrehumbert (1995), on the other hand, distinguishes in his treatment of the tropical climate between moist and dry regions and emphasizes the importance of the *bimodality* in humidity profiles associated with the two types of regions. As for the homogeneity of the temperature profiles, the origin of the bimodality in the humidity profiles is closely related to the dynamical constraints in the low-latitude atmosphere. Over the tropical oceans, large-scale ascending motion is associated with low-level convergence of humid air. These two interrelated dynamical phenomena lead to a predominantly moist, convectively active climate, in which heat is supplied mainly by the "runaway greenhouse" effect. In contrast, descending motion occurs in areas, located mainly over the subtropical land regions, where the largely inhibited surface emission acts as a regulator; such an area is generally dry.

A remarkable fact in the low-latitude atmosphere is, therefore, the apparent contradiction between the temperature profiles' spatial *homogeneity* on the one hand, and the marked *bimodality* in the spatial distribution of humidity profiles, on the other. In the Earth climate system, this distinction between the nature of radiative-convective equilibrium in tropical and subtropical areas arises, at least in part, due to the already mentioned dynamical constraints. In this study, however, we present a very simple, purely radiative model that illustrates how these two seemingly contradictory aspects of low-latitude climate can coexist at radiative equilibrium or near-equilibrium. The model results we obtain help clarify the relative role of dynamical and thermodynamical processes in the low-latitude atmosphere.

For this purpose, we use a highly idealized, single-column model with shortwave (SW) and longwave (LW) radiations; each consists of two-stream, up- and downward fluxes (Li et al. 1997). We show that the model exhibits *two* LW transmissivity profiles for *one* prescribed temperature profile and fixed insolation at the top-of-the-atmosphere. Observational evidence suggests that these two branches of the LW transmissivity relate to the bimodal humidity distribution in the low-latitude climate system. Furthermore our sensitivity analysis sheds some light on the nature of the two possible equilibria in LW transmissivity: stability of the "dry" equilibrium is found to differ from that of the "moist" equilibrium despite the identical temperature profiles associated with both. The (in)stability of the latter is associated with our model's version of the "runaway greenhouse" effect.

In order to seek analytical solutions, while concentrating on the coexistence mechanism of the temperature's homogeneity and the LW transmissivity's bimodality in the low-latitude atmosphere, we limit ourselves to the case of radiative, rather than radiative-convective, equilibrium described by the n-layer, single-column model of Li et al. (1997). Moreover we neglect energy exchanges through the tropics-extratropics lateral boundaries or air-surface interaction through the lower boundary, as a first step in examining the bimodality of the tropics' optical properties. The processes neglected at this stage are, of course, important in maintaining the tropical climate's energetics and should not be overlooked entirely. We will address these issues in the concluding remarks.

An important aspect of this study is therefore the model's ability to explicitly describe the underlying, fundamental processes in a radiative equilibrium based on its analytical solutions. The derivation of these solutions and some of their subtler properties have an intrinsic interest as well, but require a fairly detailed description, which could detract from the flow of the main arguments. We describe therefore the essence of our analysis in the main text, with as few technical details as possible. Three appendices are used to present the model solutions as well as outline their derivation and properties for the interested reader, who might want to extend the model or apply it to other climate problems.

This work is organized as follows. In Sect. 1.2, a one-layer version of our idealized model is introduced to provide the physical rationale of the present approach. The n-layer model and its basic characteristics are outlined in Sect. 2. This entire section may be omitted without significant loss of continuity, if the reader is only interested in the main physical aspects of our results and its application to atmospheric observations, which are contained in Sects. 3 and 4, respectively.

We present the observed aspects of the temperatures' homogeneity and humidities' bimodality in Sect. 3.1. The mechanisms leading to their coexistence are studied analytically in Sect. 3.2. In Sect. 3.3 we assess the stability of the temperature profile with respect to changes in the LW transmissivity for either one of the two solution branches, "moist" or "dry". Our analysis is validated against the observational data in Sect. 4. Section 5 provides the summary of our results (Sect. 5.1) and their discussion in the context of related work and

the "runaway greenhouse" effect (Sect. 5.2). A complete derivation of the model is presented in Appendix A, the complete sensitivity analysis is given in Appendix B, and the effect of latitude on the bimodality of humidity profiles is discussed in Appendix C.

1.2 Motivation: a one-layer model

Many of the ideas concerning radiative equilibrium that are studied here by using our n-layer atmospheric column model can be best understood by analyzing the simplest case, i.e., a one-layer model (e.g., James 1994). Figure 1 shows a schematic diagram of this one-layer model, in which a slab with temperature T overlies a surface layer with temperature T_0 above the ground.

The originality of our one-layer radiative model is to allow SW flux to be absorbed into the slab:

$$E = A - A_0 \ ; \tag{1}$$

here A and A_0 are the *total* downward SW fluxes at the top of the slab and surface layer, respectively, and E is therefore the *net* SW flux absorbed into the slab. The SW fluxes are determined by the slab's SW properties only, and do not depend on its LW properties. The downward LW flux at the top of the slab is denoted by I and represents LW conditions imposed by the atmosphere above. In conventional one-layer models, I is generally set to zero, since it is assumed that interplanetary space lies directly above the slab. We keep I nonzero here to preserve the similarity with the n-layer model discussed in the subsequent sections.

Radiative-equilibrium conditions are given by the energy balance in the slab and surface layer:

$$A = rQ + tr_0Q_0 - I \ , \tag{2a}$$

$$A_0 = -rQ + r_0Q_0 - tI \ . \tag{2b}$$

Here t and r are the LW transmissivity and emissivity of the slab, respectively, r_0 is the soil emissivity, and $Q = \sigma T^4$ and $Q_0 = \sigma T_0^4$ are the Stefan-Boltzmann (SB) energies that are associated with the LW radiation, while $\sigma = 5.67 \times 10^{-8}$ W m^{-2} is the SB constant. The energies Q and Q_0 are in one-to-one correspondence with the temperatures of the slab and surface layer, respectively.

LW transmissivity t is closely related to the *optical thickness* (Goody and Yung 1989; Liou 1992) and opacity (Rennó 1997) of the atmosphere. Small LW transmissivity t corresponds to an optically thick atmosphere with large opacity, while large LW transmissivity t, i.e., t close to unity, corresponds to an optically thin atmosphere with small opacity. The ratio

$$b = \frac{r}{1-t} \tag{3}$$

can be thought of as the conversion coefficient between SB and the energies available to the slab. Generally $r \simeq 1 - t$ and therefore b will be approximately constant from layer to layer and near unity (Li et al. 1997).

We first examine the characteristics of the SB energy at equilibrium. When the SW fluxes (A, E), the LW upper-air flux I and optical properties (t, r, r_0) are given, the SB energies are determined uniquely by

$$Q = \frac{1}{b}\left(\frac{1}{1+t}A_0 + \frac{1}{1-t^2}E + I\right) \ , \tag{4a}$$

$$Q_0 = \frac{1}{r_0}\left(\frac{A + A_0}{1+t} + I\right) \ . \tag{4b}$$

Next we solve for the equilibrium LW transmissivity t, assuming that other quantities are given. Equation (4a) is quadratic with respect to t:

$$(bQ - I)t^2 - A_0 t - (bQ - I - A) = 0 \ . \tag{5a}$$

Its solutions

$$t = \begin{cases} \frac{1}{2(bQ-I)}\{A_0 \pm [A_0^2 + 4(bQ-I)(bQ-I-A)]^{1/2}\}, & \text{for } Q > Q^{(c)}; \\ \frac{1}{A_0}(A - \sqrt{A^2 - A_0^2}) \equiv t^{(c)}, & \text{for } Q = Q^{(c)} \ ; \end{cases} \tag{5b}$$

are real for $Q \geq Q^{(c)}$, where

$$Q^{(c)} \equiv \frac{1}{b}\left\{\frac{1}{2}[A + (A^2 - A_0^2)^{1/2}] + I\right\} \ , \tag{5c}$$

and superscript $\{\cdot\}^{(c)}$ stands for *critical*. There are, hence, two possible solutions for the LW transmissivity t: one is larger and the other smaller than the critical LW transmissivity $t^{(c)}$ of Eq. (5b); the latter depends entirely on the SW fluxes A and A_0 from above and below the slab. Note that the model atmosphere cannot sustain radiative equilibrium if the SB energy Q becomes smaller than $Q^{(c)}$.

For a given soil emissivity r_0, we obtain from Eq. (4b) that the higher t, the smaller Q_0 will be. In other words, the optically thinner the slab is, the less SB energy will be emitted from the surface. It follows furthermore that,

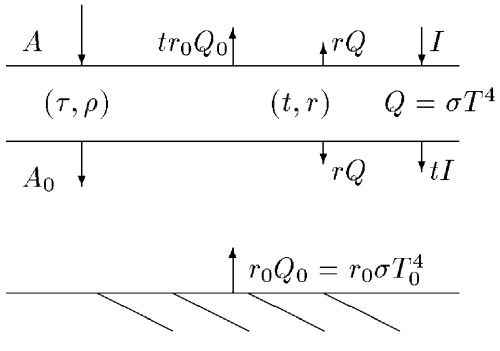

Fig. 1 One-layer model schematics for radiative equilibrium; see text and Table 1 for symbols

for a given r_0, there are not only two values of t, i.e., of optical thickness, but also two possible values of surface-air temperature $T_0 = (Q_0/\sigma)^{1/4}$.

Note that the critical SB energy $Q^{(c)}$ has, in fact, two solutions as well. We choose the one given in Eq. (5c) for physical consistency, so that the corresponding $t^{(c)}$ satisfy $0 \le t^{(c)} \le 1$; the value of $t^{(c)}$ that corresponds to the other solution is always greater than unity. The critical value $Q^{(c)}$ corresponds to the minimum temperature $T^{(c)} = (4Q^{(c)}/\sigma)^{1/4}$ of the slab, below which no radiative equilibrium can exist any longer. When Q reaches the critical value $Q^{(c)}$ from above, the two LW transmissivity solutions coincide at $t = t^{(c)}$; see Eq. (5b).

Let us demonstrate numerically the bimodality of LW transmissivities by applying Eq. (5) to a set of values corresponding roughly to Earth's present climate. We assume that the SW conditions are: $A = S(1-\alpha)/4 = 240.0$ W m^{-2} and $(A_0, E) = (0.95, 0.05)A = (227.7, 12.0)$ W m^{-2}, where $S = 1370$ W m^{-2} and $\alpha = 0.3$ (Hartman et al. 1986) are solar insolation at the top-of-the-atmosphere and planetary albedo, respectively. For simplicity we assume $I = 0$ and $b = 1$ at the top and bottom of the atmosphere, respectively, as in the conventional one-layer model, and that the surface emissivity is $r_0 = 1$. For a *reference* LW transmissivity $t = 0.6$, Eq. (4) yields a unique pair of SB energies $Q = 161.4$ W m^{-2} and $Q_0 = 292.2$ W m^{-2}; equivalently, one obtains a unique pair of temperatures for the slab ("upper air") and surface layer, $T = 230.1$ K and $T_0 = 267.9$ K.

Given this SB energy Q, we can now compute from Eq. (5) the two solutions for the LW transmissivity as $t = 0.6$ and 0.814. The former is the original *reference* value; we shall call the latter the *bifurcated* value (see Sect. 3.2 for the physical background of this terminology). The corresponding bifurcated values of Q_0 and T_0 are $Q_0 = 258.0$ W m^{-2} and $T_0 = 259.7$ K. The corresponding critical values are $Q^{(c)} = 157.3$ W m^{-2} and $t^{(c)} = 0.724$. The bifurcated solution has higher LW transmissivity and hence would correspond to a drier air mass than the reference one.

The underlying mechanism of bimodality in LW transmissivity for this simple one-layer model is the presence of the net SW flux E absorbed into the slab. When a temperature profile is obtained uniquely from the prescribed SW fluxes, E introduces the nonlinear dependence of Q on t. The rest of the study is devoted to generalizing our model and analysis from one to n layers, and to the validation of the results against the observations.

2 Analytical model

The n-layer model studied here is a slightly modified and more general version of Li et al.'s (1997) model. Figure 2 shows the schematic diagram of the generalized model. The model atmosphere's optical properties are defined in each layer i: SW optical properties are *transmissivity* τ and *reflectivity* ρ, while the LW properties are *transmissivity* t and *emissivity* r. An important difference between the present model version and Li et al.'s (1997) version is that we allow here LW emissivity r to be independent of t, while the previous version used $r \equiv 1 - t$.

The top and bottom boundaries of layer i are defined by the levels i and $i-1$, respectively; the fluxes are defined for both SW and LW radiation at these boundaries.

Each radiative component has two-way fluxes: (D, U) for SW down- and upward fluxes and (I, F) for their LW counterpart. The thermal state of each atmospheric layer is represented by the SB energy $Q = \sigma T^4/4$. The subscripts of the optical properties and fluxes correspond to the layers and levels, $0 \le i \le n$, respectively. SW surface albedo is ρ_0 and the solar insolation constant is S. A complete explanation of notation is given in Table 1.

2.1 Shortwave energy transfer

We summarize here the main characteristics of the SW radiation associated with the n-layer model. Analytical solutions are derived in Appendix A.1 where additional physical implications are discussed.

Since the SW radiation is induced by the solar forcing at the top-of-the-atmosphere, it is natural to consider the total downward SW flux A_i at level i:

$$A_i = D_i - U_i \ ; \tag{6a}$$

D_i and U_i are related to each other and to the corresponding fluxes in the layers immediately above and below by transmission and reflection processes (Li et al. 1997) as follows:

$$U_i = \rho_i D_i + \tau_i U_{i-1} \ , \tag{6b}$$

$$D_{i-1} = \tau_i D_i + \rho_i U_{i-1} \ . \tag{6c}$$

The boundary conditions are given by the solar forcing at the top and by damped reflection at the bottom:

$$D_n = \frac{S}{4}, \quad U_0 = \rho_0 D_0 \ . \tag{6d}$$

Accordingly, the total downward SW flux A satisfies the following *radiative-transfer relation*:

$$A_{i-1} - (\tau_i + \rho_i)A_i = -(1 - \tau_i - \rho_i)(U_i + U_{i-1}) \ . \tag{7}$$

In this relation, $\gamma_i \equiv (1 - \tau_i - \rho_i)$ is called the *extinction coefficient* (Goody and Yung 1989) and is known to play a key role in various radiative processes; it will be therewith a key parameter in the interpretation of our results. It acts here as a transmission coefficient for the total flux A.

2.2 Longwave energy transfer

While the solar energy received at the top-of-the-atmosphere induces the downward propagation of the total SW flux A throughout the atmosphere, the LW radiation returns the energy back to space in order to maintain the overall radiative balance in the climate system. The *outgoing longwave radiation* (OLR) measured at level i is the total upward LW flux:

$$W_i = F_i - I_i \ . \tag{8a}$$

The LW radiative-transfer relations are similar to Eqs. (6) and (7) for the SW fluxes. In the LW radiation, the reflective fluxes on the right-hand side (RHS) of Eqs. (6b, c) are replaced by emission of SB energy (see Fig. 2), while the only differences in the transmission process are the different values of the corresponding SW and LW transmissivities. Hence the LW fluxes satisfy

$$F_i = t_i F_{i-1} + r_i Q_i \ , \tag{8b}$$

$$I_i = t_{i+1} I_{i+1} + r_{i+1} Q_{i+1} \ . \tag{8c}$$

Appendix A.2 provides the analytical solution of F_i and I_i as functions of the LW optical properties (t_i, r_i) and SB energies Q_i, along with a discussion of this solution's physical implications.

The main features of the LW radiation are that the upward flux F_i depends exclusively on lower-layer properties, i.e., on (t_j, r_j) and

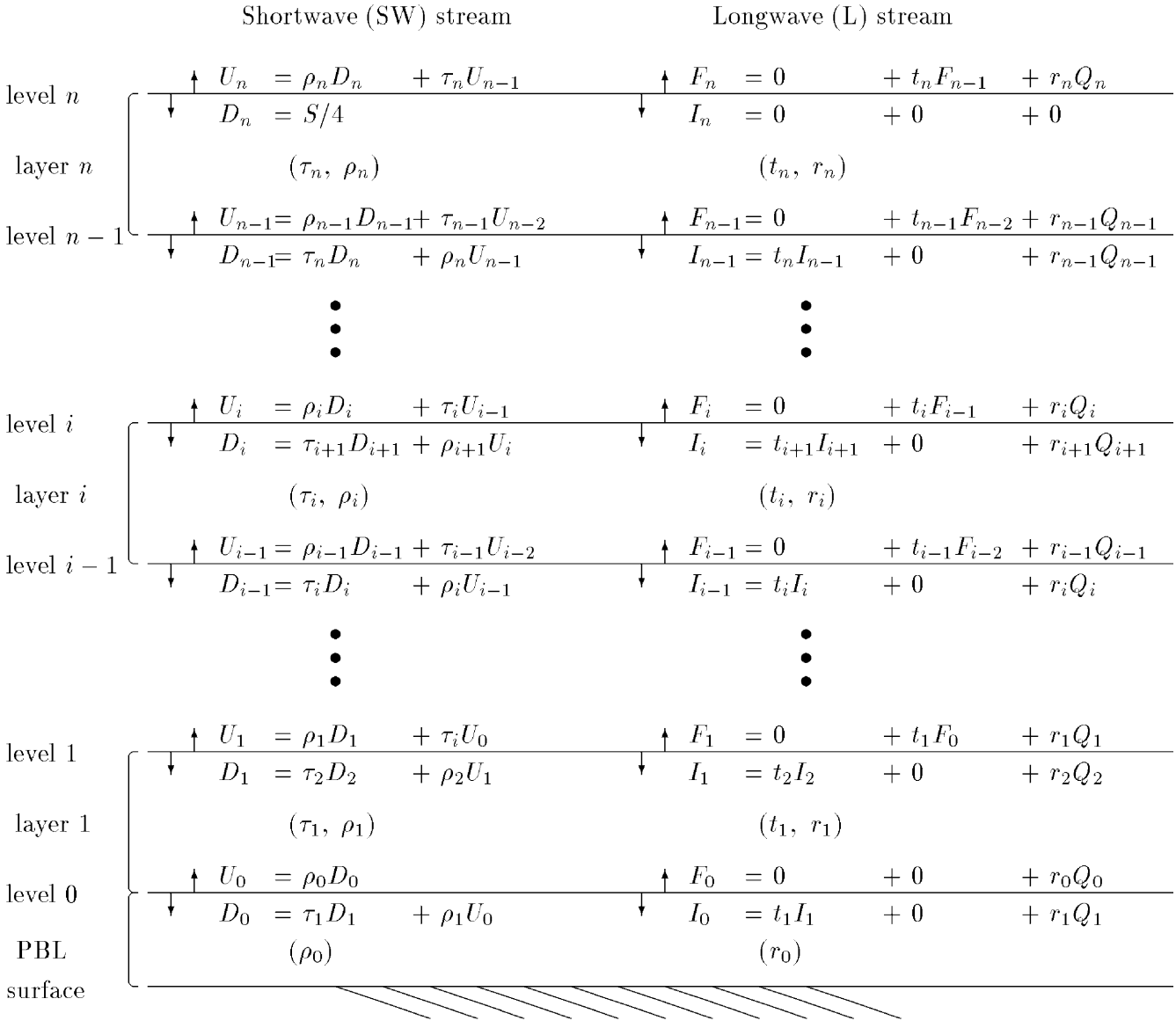

Fig. 2 Schematic diagram for n-layer model; see text and Table 1 for symbols

Q_j for $j \le i$, while the downward flux I_i depends on only upper-layer properties for $j > i$. The second terms on the RHS of Eqs. (8b) and (8c), respectively, show how the emission of SB energy from one layer becomes part of the total upward OLR, but also propagates downward so as to affect the thermal state of the atmospheric layers below. The latter is the atmosphere's *greenhouse effect*.

Equation (8) yields the *radiative-transfer relation* for the total upward LW flux:

$$W_i - t_i W_{i-1} = (1 + t_i)\{r_i Q_i - (1 - t_i) I_i\} \ . \tag{9}$$

Here $(1 - t_i)$ is the LW extinction coefficient for layer i and, like its SW counterpart, it is a crucial parameter in determining the state of radiative equilibrium.

From Eq. (9), SB energy Q_i can be expressed as:

$$Q_i = \frac{1}{b_i}\left\{\frac{1}{1 + t_i} W_{i-1} + \frac{1}{1 - t_i^2}(W_i - W_{i-1}) + I_i\right\}, \quad 1 \le i \le n \ , \tag{10a}$$

$$Q_0 = \frac{1}{r_0}\left(\frac{W_0 + W_1}{1 + t_1} + I_1\right) \ , \tag{10b}$$

where:

$$b_i = \frac{r_i}{1 - t_i} \tag{11}$$

is a conversion coefficient between Q_i and available energy in each layer (see Sect. 1.2). The SB energy Q_i consists of three distinct contributions: the OLR contribution from below (W_{i-1} term), the local contribution within the layer ($W_i - W_{i-1}$ term), and the contribution from the atmospheric layers above (I_i term). There is a strong similarity between Eqs. (4) and (10). In Sect. 3.2, we shall see how the bimodality of LW transmissivities that arises for the one-layer model of Sect. 1.2 out of Eq. (4) will likewise arise out of Eq. (8) for a full n-layer transmissivity profile.

2.3 Radiative processes at equilibrium

In a radiative-equilibrium model one considers the energy balance between the SW and LW radiation. In terms of the *total* fluxes at *level i*, the balance is:

Table 1 A glossary of the principal symbols used in this study: SW and LW properties (upper panel) and bifurcation properties (lower panel)

	Symbol		Definition
	Shortwave (SW)	Longwave (LW)	
Optical parameters	τ	t	Transmissivity
	ρ	r	Reflectivity
	α & ρ_0	–	Planetary and surface albedos
	γ	–	Extinction coefficient
	–	b	Conversion ratio
	U	F	Upward at a given level
	D	I	Downward at a given level
Flux/ energy	A	W	Total at a given level
	E	H	Net in a given layer
	ε	–	Relative net in a given layer
	S	–	Insolation
	–	Q	Stefan-Boltzmann energy
Other	–	σ	Stefan-Boltzmann constant
	–	T	Temperature
	–	h	Humidity
	Symbol		Definition
Branch type	$\{\cdot\}^{(b)}$		Bifurcated
	$\{\cdot\}^{(d)}$		Dry
	$\{\cdot\}^{(g)}$		Greenhouse
	$\{\cdot\}^{(m)}$		Moist
Bifurcation condition	$\{\cdot\}^{(c)}$		Critical value
	$\{\cdot\}^{(c)}_{*}$		Intersection of reference and critical profiles

$$A_i = W_i \ , \tag{12}$$

while in terms of the *net* fluxes into each *layer*:

$$E_i = H_i \ ; \tag{13}$$

here

$$E_i \equiv A_i - A_{i-1} = \gamma_i (D_i + U_{i-1}) \ , \tag{14a}$$

$$H_i \equiv W_{i-1} - W_i = (1 - t_i)(I_i + F_{i-1}) - 2 r_i Q_i \ . \tag{14b}$$

The difference between Eqs. (12) and (13) consists in the fact that Eq. (13) allows, in principle, a constant SW flux to run through the column, and be matched by an equal and opposite LW flux. In the present model, we take for simplicity this arbitrary additive constant to be zero. It is possible, however, as done for instance by Hu and Randall (1994) in their numerical model, to allow this height-independent flux to depend on time, and be balanced by changes in the heat stored by the ocean mixed layer.

The net SW flux E_i in Eq. (14a) is the total incoming SW flux $(D_i + U_{i-1})$ into the layer i, attenuated by the extinction coefficient γ_i; it depends on the SW conditions $(\vec{\tau}, \vec{\rho}, \rho_0; S)$ only. The net LW flux H_i consists of the total incoming LW flux $(I_i + F_{i-1})$, attenuated by the corresponding extinction coefficient $(1 - t_i)$, minus the SB energy $2 r_i Q_i$ emitted into the adjacent layers; H_i depends on the LW conditions $(\vec{t}, \vec{r}; \vec{Q})$ only. For the sake of conciseness, we denote hereafter the complete profiles of optical properties by vectors $\vec{\tau}$, $\vec{\rho}$, $\vec{t}$, and $\vec{r}$, as in Li et al. (1997), e.g., $\vec{\tau} \equiv (\tau_1, \ldots, \tau_n)^{\mathrm{T}}$. We use the vector notation for the flux and energy profiles as well.

Because $\vec{I}$ and $\vec{F}$ are linear in $\vec{Q}$ (see Appendix A.2), Eq. (14) leads to an analytical expression of $\vec{Q}$ by solving the matrix equation

$$\vec{Q} = \mathbf{L}(\vec{t}, \vec{r}) \vec{E}(\vec{\tau}, \vec{\rho}, \rho_0; S) \ . \tag{15a}$$

The roles of the SW and LW radiative fluxes in determining SB energy $\vec{Q}$, and therefore the temperature profile $\vec{T}$, with $T_i = (4 Q_i / \sigma)^{1/4}$, is clear in this form: The SW radiation deposits net flux $\vec{E}(\vec{\tau}, \vec{\rho}, \rho_0; S)$ into each layer, while the LW radiation then redistributes the energy throughout the atmosphere by means of direct propagation and emission (see discussion in Sects. 2.1 and 2.2).

The redistribution process is represented by the $(n+1) \times (n+1)$ matrix $\mathbf{L}$ whose elements L_{ij} are:

$$L_{ij} = \begin{cases} \frac{1}{b_i} \left(\frac{1}{1+t_i} + \sum_{l=i+1}^{n \geq i+1} \frac{1-t_l}{1+t_l} \right), & \text{for } i > j; \\ \frac{1}{b_i} \left(\frac{1}{1-t_i^2} + \sum_{l=i+1}^{n \geq i+1} \frac{1-t_l}{1+t_l} \right), & \text{for } i = j; \\ \frac{1}{b_i} \left(\frac{1}{1+t_j} + \sum_{l=j+1}^{n \geq j+1} \frac{1-t_l}{1+t_l} \right), & \text{for } i < j \ . \end{cases} \tag{15b}$$

The elements L_{ij} depend nonlinearly on the LW transmissivities $\vec{t}$. The most crucial nonlinearity lies in the $1/(1 - t_i^2)$ factor for the diagonal terms $i = j$. This is the nonlinearity captured by the one-layer model of Sect. 1.2. In Sect. 3, we show how this nonlinearity will lead to the bimodal solution branch of LW transmissivity t for a prescribed SB energy Q in detail, along with the stability associated with them. A complete description of redistribution matrix $\mathbf{L}$'s properties is provided in Appendix A.3.

In order to demonstrate the main radiative processes responsible for determining the Earth atmosphere's temperature profile, we apply the n-layer model to compute SB energy $\vec{Q}$. The optical properties used here were obtained from the 11-layer atmospheric general circulation model (GCM) of the Laboratoire de Météorologie Dynamique (LMD: Li et al. 1997). They correspond to its clear-sky case and are given in Table 2. For simplicity, the conversion coefficient b is set equal to unity. Table 3 shows each element of $\vec{Q}$, $\mathbf{L}$ and $\vec{E}$ for $S_0 = 1370$ W m^{-2} and $\rho_0 = 0.3$.

The qualitative behavior of the SB energy profile $\vec{Q}$ computed by our 11-layer model is quite similar to that observed in the real, as well as in the GCM-simulated, atmosphere. The values of SB energy $\vec{Q}$, and hence of the temperature $\vec{T}$, decrease from the top-of-the-atmosphere to a minimum at the tropopause level and increase towards the Earth's surface, where they exceed the value at the top.

Based on the form of the redistribution matrix $\mathbf{L}$ given by Eq. (15), along with the numerical values of its entries and of the E- and Q-profiles in Table 3, we can draw certain physical conclusions about our model results. There are three major processes that are responsible for the present climate's SB energy profile Q, and hence for its temperature profile. First, the net SW flux E_i is governed by

Table 2 Optical parameters obtained from LMD's GCM; layer 11 is in the upper stratosphere and layer 1 is near the Earth surface. See text and Table 1 for symbols and Li et al. (1997) for further details

Layer		SW		LW		Extinction	
i	(hPa)	τ	ρ	t	r	$1-\tau-\rho$	$1-t$
11	(15)	0.9720	0.0054	0.9630	0.0370	0.0226	0.0370
10	(73)	0.9897	0.0053	0.9765	0.0235	0.0050	0.0235
9	(152)	0.9874	0.0078	0.9486	0.0514	0.0048	0.0514
8	(274)	0.9773	0.0113	0.8468	0.1532	0.0114	0.1532
7	(416)	0.9587	0.0151	0.7255	0.2745	0.0262	0.2745
6	(573)	0.9522	0.0161	0.6633	0.3367	0.0317	0.3367
5	(718)	0.9572	0.0143	0.6428	0.3572	0.0285	0.3572
4	(841)	0.9635	0.0113	0.6163	0.3837	0.0252	0.3837
3	(926)	0.9754	0.0072	0.6578	0.3422	0.0174	0.3422
2	(980)	0.9868	0.0038	0.7756	0.2244	0.0094	0.2244
1	(1004)	0.9930	0.0020	0.8724	0.1276	0.0050	0.1276

Table 3 Individual components of the matrix equation $\mathbf{L}\vec{E} = \vec{Q}$ when using optical parameter values from Table 2 with $S = 1370$ W m^{-2} and $\rho_0 = 0.3$, as in Li et al. (1997)

Layer	L_{ij}												E_i	Q_i
i	11	10	9	8	7	6	5	4	3	2	1	0		
11	13.77	0.51	0.51	0.51	0.51	0.51	0.51	0.51	0.51	0.51	0.51	0.51	9.72	259.4
10	0.51	21.55	0.52	0.52	0.52	0.52	0.52	0.52	0.52	0.52	0.52	0.52	2.12	178.9
9	0.51	0.52	10.01	0.54	0.54	0.54	0.54	0.54	0.54	0.54	0.54	0.54	2.00	158.0
8	0.51	0.52	0.54	3.59	0.60	0.60	0.60	0.60	0.60	0.60	0.60	0.60	4.67	166.3
7	0.51	0.52	0.54	0.60	2.25	0.72	0.72	0.72	0.72	0.72	0.72	0.72	10.52	197.2
6	0.51	0.52	0.54	0.60	0.72	2.08	0.90	0.90	0.90	0.90	0.90	0.90	12.31	236.7
5	0.51	0.52	0.54	0.60	0.72	0.90	2.21	1.11	1.11	1.11	1.11	1.11	10.66	278.9
4	0.51	0.52	0.54	0.60	0.72	0.90	1.11	2.33	1.34	1.34	1.34	1.34	9.13	322.8
3	0.51	0.52	0.54	0.60	0.72	0.90	1.11	1.34	2.72	1.56	1.56	1.56	6.15	364.2
2	0.51	0.52	0.54	0.60	0.72	0.90	1.11	1.34	1.56	3.67	1.73	1.73	3.27	394.8
1	0.51	0.52	0.54	0.60	0.72	0.90	1.11	1.34	1.56	1.73	5.47	1.82	1.72	412.8
0	0.51	0.52	0.54	0.60	0.72	0.90	1.11	1.34	1.56	1.73	1.82	2.36	184.02	504.8

the extinction coefficient γ_i for $1 \le i \le n$ and has a pronounced minimum at tropopause level; hence very little SW flux is available there for local conversion into SB energy. The key role played by this parameter underlines the importance of the current debate about the actual level of atmospheric absorption and the success of atmospheric GCMs in simulating it, known as the "anomalous absorption" debate (Cess et al. 1995; Kato et al. 1997; Johnson and Ciesielski 2000).

Second, the surface value E_0 is much larger than all upper-air E_i's, due to the much higher value of the "co-albedo" $(1-\rho_0)$ as compared to the extinction coefficients γ_i. Upward redistribution of E_0 via L_{0i} into atmospheric layer i decreases monotonically with the height of the layer i. This leads to a decrease of Q_i from the surface to the tropopause. Finally, above the tropopause, local conversion into SB energy is very efficient due to the higher t_i values in the lower stratosphere, and so the temperatures can increase again.

3 Bimodality: observations and analysis

In this section, we first present the observational characteristics of the low-latitude climate system focusing on the spatial homogeneity of the temperature profiles and bimodality of humidity profiles. We then illustrate analytically, using our n-layer, single-column model, how these apparently contradictory features can coexist at radiative equilibrium or near it, even in the absence of explicit small-scale vertical or large-scale horizontal air flow.

3.1 Observational evidence

To illustrate the opposite characteristics of homogeneity in temperatures and bimodality in humidity and LW optical properties, observed vertical profiles of temperature, humidity and optical properties were computed for the three low-latitude regions shown in Fig. 3. The region in the western Equatorial Pacific (marked Box 1 in the figure) corresponds to the humid, ascending branch of the Walker circulation over the warm pool of water associated with the Maritime Continent. The other two regions (marked Boxes 2 and 3) are in subsidence areas associated with the descending branches of the Walker and Hadley circulations, to wit, the eastern tropical Pacific (Box 2) and the subtropical North Pacific (Box 3), respectively; therefore these regions are generally drier than their surroundings. Box 1 corresponds roughly to Pierrehumbert's (1995) *furnace* and we expect it to be subject to a runaway greenhouse effect, while Boxes 2 and 3 correspond to his *radiator fins* (see Fig. 7 in Pierrehumbert 1995).

The vertical profiles of the atmospheric properties for the three regions shown in Fig. 3 were computed from the European Centre for Medium-Range Weather Forecasts (ECMWF) reanalysis data. The values are annual means over each region. To convert the reanal-

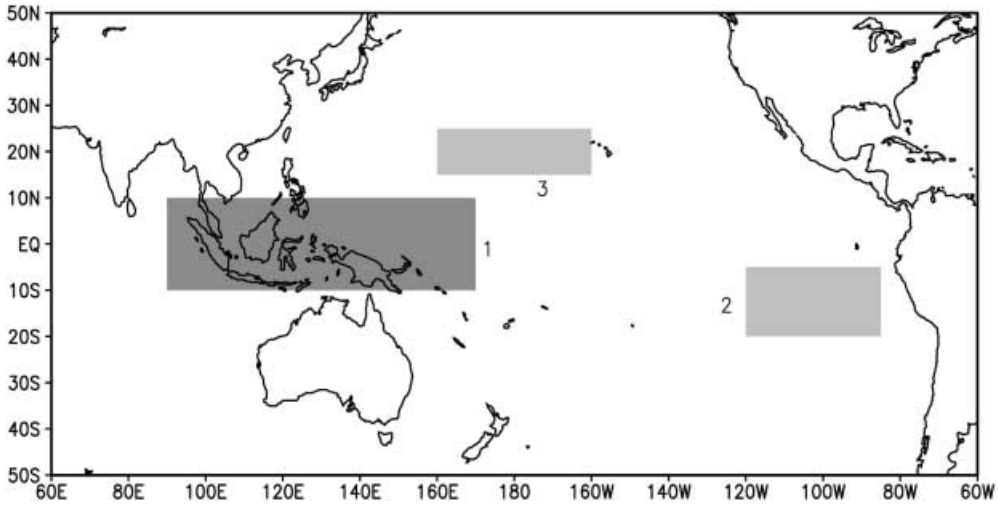

Fig. 3 Three regions used to convert the ECMWF reanalysis data into optical properties: Box 1 (*dark shading*) is a moist region and Boxes 2 and 3 (*light shading*) are dry regions

ysis data into atmospheric optical properties, the following two steps were taken: we first computed SW and LW fluxes from the reanalysis using Morcrette's (1991) advanced and detailed column model, and then fitted Li et al.'s (1997) simple model to these fluxes to obtain the optical properties. The layer depths used for the conversion are plotted in Fig. 4a.

The observed profiles of temperature T and humidity h together capture the coexistence characteristics well. The mean temperature profiles of the three regions are strikingly similar, as shown in Fig. 4b; this confirms their well-known homogeneity throughout the low-latitude atmosphere. Their qualitative behavior is the same as for the GCM results described in Sect. 2.3.

The mean humidity profiles in Fig. 4c all show the monotonic decrease with altitude known from observations and GCM simulations, as well as a very dry upper troposphere. There are, however, clear differences between the moist and dry regions in the lower and middle troposphere. These features agree well with the overall bimodality of humidity profiles in low latitudes.

Among the atmosphere's optical properties, LW transmissivity t is strongly correlated with humidity h at a given altitude: the higher the humidity, the lower the LW transmissivity, and thus the higher the LW opacity; this in turn leads to a more efficient greenhouse effect (Rennó 1997). Accordingly the three LW transmissivity profiles also exhibit a distinct dependence on the region, i.e., whether the upper air is moist or dry (Fig. 4d). The qualitative behavior is quite similar from one t-profile to another, as is the case for the humidities. Typically LW transmissivity has a high value in the middle atmosphere, with a maximum around 50 hPa, and decreases fairly regularly as the altitude goes down till 850 hPa, from where it gently increases towards the Earth's surface.

Notice that the bimodality that manifests itself in quantitative differences among LW transmissivity t and humidity h profiles arises only at and below tropopause level; differences in the lower stratosphere are quite minor.

It is worth mentioning that the profiles of SW optical properties $(\vec{\tau}, \vec{\rho})$ show no systematic dependence on moist or dry region, although individual profiles are fairly different from each other (see Fig. 4e, f). The SW extinction coefficient profiles $\vec{\gamma}$ of the three regions (not shown in the figure), however, exhibit a common structure that resembles that of our globally averaged model's extinction coefficients in Table 2, based on the LMD's GCM simulation.

3.2 Bimodality of the longwave transmissivity

In Section 1.2, the one-layer model was used to explain how the net SW flux E absorbed into the slab gives rise to nonlinearity in the radiative equilibrium state, due to the SW net flux E's quadratic dependence on LW transmissivity t. This quadratic nonlinearity leads to two possible solutions for the LW transmissivity t, given a prescribed SB flux Q or temperature T and SW conditions. We generalize in this section our results to the n-layer model. These results are then used to help explain the observed characteristics of the low-latitude climate, i.e., the bimodality of tropospheric humidities and LW transmissivities subject to the temperatures' homogeneity.

We prescribe the SW optical properties so as to obtain a realistic radiative equilibrium. As explained in Sect. 2.2, this can be done in our model independently of the LW property values. Doing so allows us to focus on the role of humidity, which only affects the LW radiative transfer.

We saw in Sect. 2.3 that energy balance between the SW and LW radiative fluxes can be imposed between total fluxes A_i and W_i at each level or between net fluxes E_i and H_i into each layer; see Eqs. (12) and (14), respectively. Using these balances in Eq. (10) for the SB fluxes, we obtain:

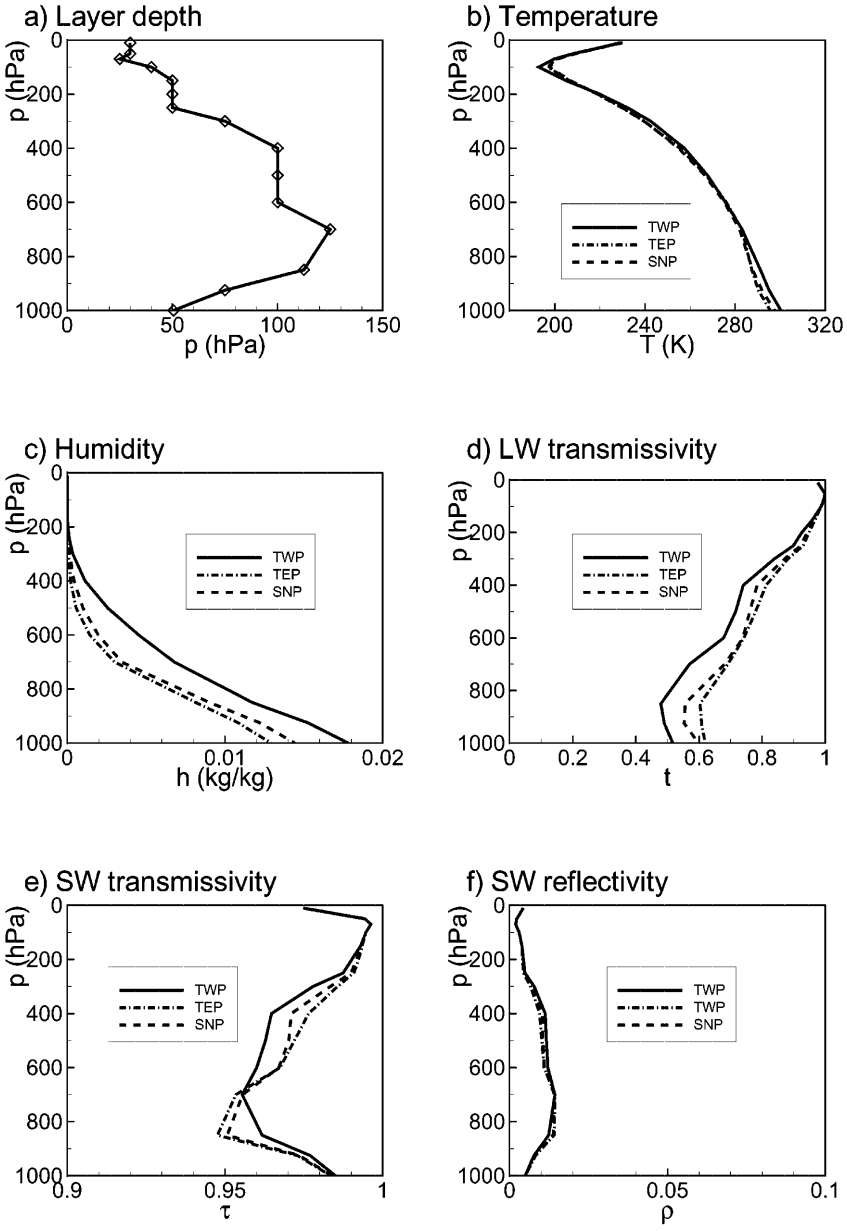

Fig. 4a–f Vertical profiles of optical properties and other variables in the three regions shown as Boxes 1–3 in Fig. 3 (*solid*, *dashed*, and *dashed-dotted lines*, also marked *TWP*, *TEP*, and *SNP*, respectively, for tropical Western Pacific, tropical Eastern Pacific, and subtropical Northern Pacific), obtained from the ECMWF reanalysis data: **a** layer depth used to convert reanalysis data to radiative properties, **b** temperature T; **c** humidity h; **d** LW transmissivity t; **e** SW transmissivity τ; and **f** SW reflectivity ρ

$$Q_i = \frac{1}{b_i}\left(\frac{1}{1+t_i}A_{i-1} + \frac{1}{1-t_i^2}E_i + I_i\right), \quad \text{for } i \geqslant 1 \ ; \quad (16a)$$

$$Q_0 = \frac{1}{r_0}\left(\frac{A_1 + A_0}{1+t_1} + I_1\right) \ . \quad (16b)$$

This is a generalization of Eq. (4) for the one-layer model discussed in Sect. 1.2. Usually the conversion coefficients b_i are constant and near unity. The three terms on the RHS of Eq. (16a) are the contributions to Q_i from the layers below (A_{i-1} term), the layer itself (E_i term), and the layers above (I_i term), respectively.

As in the case of the one-layer model, Eq. (16) yields a quadratic equation for t_i similar to Eq. (5a). Because I_i is a function of the LW transmissivities t_j of the higher layers ($j > i$) only (see Appendix A.2), t_i can be solved sequentially from the top ($i = n$) to the bottom ($i = 1$) for a prescribed temperature profile $\vec{Q}$ and SW conditions ($\vec{A}$, $\vec{E}$) under the assumption that b_i is a constant (see Sect. 1.2):

$$t_i = \begin{cases} \frac{1}{2(b_iQ_i - I_i)}\{A_{i-1} + [A_{i-1}^2 - 4(b_iQ_i - I_i)(b_iQ_i - I_i - A_i)]^{1/2}\}, & \text{for } Q_i > Q_i^{(c)}, \\ \frac{1}{A_{i-1}}[A_i - (A_i^2 - A_{i-1}^2)^{1/2}] \equiv t_i^{(c)}, & \text{for } Q_i = Q_i^{(c)} \ ; \end{cases} \quad (17)$$

here $Q_i^{(c)}$ is the critical SB value:

$$Q_i^{(c)} \equiv \frac{1}{b_i}\left\{\frac{1}{2}[A_i + (A_i^2 - A_{i-1}^2)^{1/2}] + I_i\right\} \ . \tag{18}$$

There exist, therefore, *two* solutions of t_i for *each* prescribed Q_i and SW conditions ($i \geq 1$), provided $Q_k \geq Q_k^{(c)}$ at each level k above the level i of interest, and $Q_i > Q_i^{(c)}$. We denote the two LW transmissivity solutions by $t_i^{(m)}$ and $t_i^{(d)}$ to represent moist and dry conditions. They satisfy the inequality

$$t_i^{(m)} \leq t_i^{(c)} \leq t_i^{(d)} \ , \tag{19}$$

where the critical LW transmissivity $t_i^{(c)}$ is a function of SW optical properties only, as in Eq. (17). When SB energy Q_i reaches its critical value, i.e., $Q_i = Q_i^{(c)}$, the two LW transmissivity solutions coincide at their corresponding critical value $t_i^{(m)} = t_i^{(c)} = t_i^{(d)}$.

Once again, as in the one-layer model, $Q_i^{(c)}$ itself has two solutions and we choose the one for which $0 \leq t_i^{(c)} \leq 1$ is satisfied. The critical value $Q_i^{(c)}$ is associated with the minimum temperature that the layer i can attain when the model atmosphere is in radiative equilibrium. Note that, as in Sect. 1.2, given the soil emissivity r_0, Eq. (16b) yields the SB flux Q_0 – and hence surface-air temperature T_0 – that matches t_1, and vice-versa.

To help explain why bimodality is observed only in the lower atmosphere, we examine the nature of the solutions of Eq. (17), solved sequentially from the top-of-the-atmosphere downward. Mathematically, the n-layer "discrete" model can admit up to 2^n-solutions for $\vec{t}$, given the SB energies $\vec{Q}$, as illustrated in Fig. 5. Observed atmospheric profiles, however, have physical continuity and therefore the vertical profile of LW transmissivity t should be a continuous function of the height coordinate. Moreover, the observed atmospheric humidity above the tropopause is near zero (see Fig. 4c) and hence the LW transmissivity there should correspond to $t_n^{(d)}$.

A set of solutions starting from $t_n^{(d)}$ has to stay therefore on the "dry" branch as we go down from layer to layer. A possible switch from the dry to moist branch can occur only when the solution achieves $t_i = t_i^{(c)}$ – and so $Q_i = Q_i^{(c)}$ – in some layer, say $i_*^{(c)}$, where the two solutions coincide with each other. Below such a layer in the atmosphere, a single prescribed Q-profile can support the two branches of solutions – $t_i^{(m)}$ and $t_i^{(d)}$ ($i < i_*^{(c)}$) – that have continuous vertical profiles throughout the atmosphere, leading to bimodality of t. We may refer to this phenomenon as "forking" of the LW transmissivity profile at the tropospheric layer $i_*^{(c)}$, with a unique t-profile above and two distinct ones below.

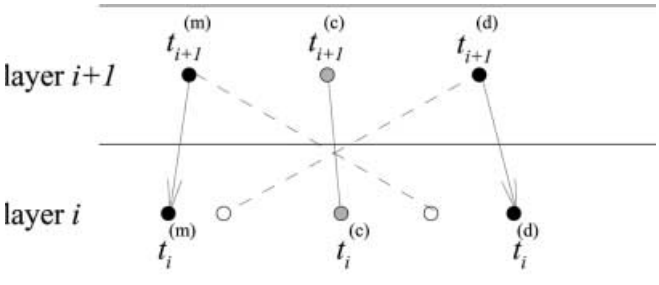

Fig. 5 Schematics for the 2^n possible sets of LW transmissivity profiles. The *gray open circles* denote the unique t-profile associated with the critical SB values $Q^{(c)}$; the *solid black circles* indicate the two extreme t-profiles chosen, dry and moist; and the *open circles* with *no shading* correspond to the additional, mathematically possible t-profiles (see text for details)

In spite of its great simplicity, our model describes the way in which the atmosphere adapts its optical properties to match the incoming solar radiation by an equal outgoing LW flux, for a given vertical temperature profile. In this interpretation, the bimodality of t when $Q > Q^{(c)}$ is the manifestation of a *bifurcation*: if the temperature profile is imposed by the dynamical and thermodynamical constraints that lead to its homogeneity throughout the tropics, then the response of the tropical atmosphere to changing conditions at the top does present a bifurcation point in its optical properties.

This bifurcation is distinct from the one found by Li et al. (1997) due to the nonlinearity of surface albedo; it may be more closely related to that found by Rennó (1997) in the sense that our nonlinearity is also associated with the hydrologic cycle. The two equilibria in Rennó (1997) correspond to the temperature profiles of an optically thin and thick atmosphere, respectively; these two may in turn correspond to our dry and moist t-profile. The exact relationship between Rennó's (1997) bifurcation in his radiative-convective, time-dependent model and ours in the present radiative-equilibrium model, however, is left for future investigations.

As in the one-layer model of Sect. 1.2, the nonlinearity at the heart of our n-layer model's bifurcation is related to the availability of a net SW flux E. Here we examine the role of this absorbed flux E further and explore what conditions favor the bifurcation's occurrence.

The critical LW transmissivity $t_i^{(c)}$ defined in Eq. (17) depends only on SW, and not on LW, conditions; it can be rewritten as follows:

$$t_i^{(c)} = \varepsilon_i + 1 - (\varepsilon_i^2 + 2\varepsilon_i)^{1/2} \ . \tag{20a}$$

Here

$$\varepsilon_i \equiv \frac{E_i}{A_{i-1}} = \gamma_i \frac{D_i + U_{i-1}}{A_{i-1}} \tag{20b}$$

is the *relative net* SW flux, which is of $\mathcal{O}(\gamma_i)$ with respect to the *total* flux. As anticipated in Sect. 1.2, the SW extinction coefficient γ_i is a major controlling factor in the subsequent analysis, via its effect on ε_i.

It is easily shown that the maximum of $t_i^{(c)}$ equals 1 at $\varepsilon_i = 0$ because $\partial t_i^{(c)}/\partial \varepsilon_i < 0$ for $\varepsilon_i \geq 0$. For an LW transmissivity profile starting on the dry branch $t_n = t_n^{(d)}$ ($t_n^{(c)} < t_n^{(d)} < 1$) at the top, the SW condition that favors the downward forking into the two branches of solutions in the lower atmosphere is therefore $\varepsilon_i \simeq \gamma_i \simeq 0$, because then $t_i^{(c)} \simeq t_i^{(d)}$. If this is the case, $t_i^{(c)}$ is more

accessible from the $t_i^{(d)}$-branch. This SW condition is likely to occur where the SW extinction coefficient γ_i is near zero, i.e., around the tropopause.

Once $\vec{\varepsilon}$ is determined from the SW conditions, the LW transmissivity can further contribute to the forking as its values decrease from near unity at the top-of-the-atmosphere toward the lower layers, where humidity is no longer negligible. Consequently, LW transmissivity t may intersect $t^{(c)}$ just below the tropopause, where these SW and LW conditions are both satisfied. For the present Earth climate, this combination of circumstances may thus lead to forking of a moist from a dry profile in the upper troposphere.

The condition $\varepsilon_i = 0$, or equivalently $E_i = 0$, generalizes the conventional one-layer model to our n-layer model by suppressing the nonlinearity of Q_i in Eq. (16). Therefore only one solution for t exists in this case:

$$t_i^{(g)} = \frac{A_{i-1}}{b_i Q_i - I_i} - 1 \quad . \tag{21}$$

We denote this unique solution by the superscript $\{\cdot\}^{(g)}$ for conventional "greenhouse model." Clearly $t_i^{(g)}$ corresponds to the $t_i^{(m)}$-branch of our model, because $t_i^{(g)} < t_i^{(c)} \equiv 1$; it is the branch explored by earlier models that considered small radiative or radiative-convective perturbations of the globally or zonally averaged temperature profiles. We discuss next the stability of the SB energy profile $\vec{Q}$ associated with the two branches, dry and moist, of LW transmissivity profiles.

3.3 "Runaway greenhouse" effect

The nonlinear dependence of the SB energies $\vec{Q}$ on the LW transmissivities $\vec{t}$, as described in Eq. (16), naturally raises a few questions concerning the stability of tropical climates, even in the absence of dynamical processes: (1) how is the SB energy profile, and hence the temperature profile, influenced by the perturbation of LW transmissivity from equilibrium; (2) is the influence similar or different for the two equilibrium profiles; and (3) how does the nonlinear relationship between humidity and temperature affect climate stability? In this section, we address the first two questions by examining the fundamental characteristics of the model's sensitivity matrix, obtained by computing the partial derivatives of the SB energies Q_i with respect to the LW transmissivities t_j. This computation is carried out along either one of the two solution branches of LW transmissivity separately; in doing so, note that $\vec{Q}$ is no longer prescribed here, as it was in Sects. 2 and 3.2.

We follow the approach introduced by Li et al. (1997) and examine first, based on the model's sensitivity matrix, how the SB energy fluxes maintain the equilibrium. Our analysis is applied next to observed atmospheric profiles, and we find that a "runaway greenhouse" effect occurs for the moist profiles. Our discussion here is limited mainly to local sensitivity within each layer, i.e., we examine only the diagonal entries $\partial Q_i/\partial t_i$ of the matrix. A complete analysis of the sensitivity matrix $\partial Q_i/\partial t_j$ and additional physical implications are presented in Appendix B.

To examine the diagonal of the sensitivity matrix, it helps to inspect the three terms on the RHS of Eq. (16) separately. The first two depend nonlinearly on t_i. The contributions from these two terms work against each other, as follows. As t_i increases, the contribution from the lower atmosphere (A_{i-1} term) is reduced, and so Q_i decreases, i.e., $\partial Q_i/\partial t_i < 0$. As t_i approaches $t_i^{(c)}$, the local, self-warming contribution (E_i term) becomes more important and eventually these two contributions balance at $t_i = t_i^{(c)}$, where $\partial Q_i/\partial t_i = 0$. The local contribution then increases rapidly as t_i approaches unity, i.e., $\partial Q_i/\partial t_i \gg 0$. Overall, $\partial Q_i/\partial t_i < 0$ along the moist branch, where $t_i^{(m)} < t_i^{(c)}$, while $\partial Q_i/\partial t_i > 0$ along the dry branch, where $t_i^{(c)} < t_i^{(d)}$. Thus the moist and dry radiative-equilibrium solutions have opposite stability properties.

To see how this mechanism might work in the Earth's atmosphere, we consider the following. As temperature T, and hence SB energy Q, increases near the surface, upper-air convection is triggered or enhanced and moisture is lifted into the troposphere. Higher humidity then lowers the LW transmissivity t (see discussion in Sect. 3.1). On the moist branch, Q rises further due to the negative sensitivity, as we just saw. Hence the moist solution branch is unstable due to a positive feedback mechanism that is our model's version of the well-known "runaway greenhouse" effect (Simpson 1927; Komabayasi 1967; Ingersoll 1969).

Our model's dry branch, on the contrary, is stable because of the positive sensitivity of Q to t that leads to a negative feedback. Roughly speaking, the stability of an air mass's temperature and humidity profile can therefore be assessed by comparing its t_i with respect to $t_i^{(c)}$; the latter is determined solely by the relative net SW flux ε_i.

For the conventional case in which the nonlinear local conversion is suppressed ($E_i \equiv 0 \equiv \varepsilon_i$), only one LW transmissivity profile exists and it corresponds to our moist branch (see Sect. 3.2). The instability of this profile is consistent with the conventional greenhouse effect.

The observed prevalence of bimodality in humidity and LW transmissivity profiles has a marked latitudinal dependence, being restricted to the tropics and subtropics (see Sect. 3.1). It is thus inseparable in the observations from the presence and dynamical effects of the Hadley and Walker cells. The meridional confinement of the Hadley cell on Earth is due to a number of complementary, dynamical and thermodynamical processes (Ghil and Childress 1987; James 1994). Even so, it is interesting to note that simple energy constraints also tend to limit this bimodality to high insolation values, and therefore to low latitudes: the forking conditions we have derived are less likely to be satisfied at high latitude, where in fact dry profiles tend to prevail, on average. This latitude dependence of the bifurcation

condition is derived in detail from our radiative-equilibrium considerations in Appendix C.

4 Application to the low-latitude atmosphere

We now validate the proposed bifurcation mechanism that leads to bimodal humidity profiles in low latitudes by using a set of observed atmospheric properties. The following steps are taken for this purpose.

1. Using the ECMWF reanalysis data averaged over the tropical Pacific warm pool area (see Box 1 in Fig. 3), we compute the reference profiles of SW properties $(\vec{\tau}, \vec{\rho}, \rho_0; S)$ and LW properties $(\vec{t}, \vec{r})$, based on the methodology described in Sect. 2.3.
2. By applying our model to the reference profiles so obtained, we compute other reference conditions such as the SW fluxes $(\vec{A}, \vec{E})$ and LW fluxes $(\vec{I}, \vec{F})$, as well as the SB energy profile $\vec{Q}$.
3. Using these reference conditions, we solve for the critical values $t^{(c)}$ and $Q^{(c)}$ in each layer.
4. We compare the reference LW transmissivity t to $t^{(c)}$ in each layer, so as to determine the type of the reference profile, dry or moist, and check whether the bifurcation condition is satisfied.
5. If the reference value t satisfies the bifurcation condition $Q_i \geq Q_i^{(c)}$ in a layer, $i = i_*^{(c)}$, we compute another solution branch, dry or moist, below the critical layer $i^{(c)}$, and call it the bifurcated solution $t^{(b)}$, with superscript $\{\cdot\}^{(b)}$ for bifurcated.
6. We compute the sensitivity $(\partial\vec{Q}/\partial\vec{t})$ along both the reference and bifurcated profiles and assess the stability of $\vec{Q}$ along both solution branches.

Figure 6a shows the reference profile of LW transmissivity $\vec{t}$; note that Tables 2 and 3 use $n = 11$, the number of layers in LMD's GCM, while in this section we use the 15 layers of ECMWF's reanalysis data (step 1). We assume in step 1 here that $b_i \equiv 1$ in Eq. (11), for the sake of simplicity. This assumption is particularly critical near the tropopause, where $t \simeq 1$ (see Fig. 4d) and so, to obtain a smooth profile of SB energies Q and avoid therewith singularities in solving Eq. (17) for t, we reduced the observed t-values in Fig. 4d by about 1% in layers 13 and 14, to yield the values shown in Fig. 6a.

The SW transmissivities $\vec{\tau}$ and reflectivities $\vec{\rho}$ are shown in Fig. 4e, f, respectively. The reference profiles of the SW and LW extinction coefficients, $\vec{\gamma} = (1 - \vec{\tau} - \vec{\rho})$ and $(1 - \vec{t})$, are plotted in Fig. 6b; the near-tropopause minimum of $\vec{\gamma}$, as well as the small values of $(1 - \vec{t})$ in the stratosphere, are apparent in the figure. Profiles of the corresponding reference conditions, for SW fluxes $(\vec{D}, \vec{U})$ and LW fluxes $(\vec{I}, \vec{F})$, SB energies $\vec{Q}$ and temperatures $\vec{T}$, are shown in Fig. 7a–d, respectively (step 2). Surface albedo and soil emissivity are taken to be $\rho_0 = 0.3$ and $r_0 = 1$ in this demonstration (see also Li et al. 1997). It is clear from Fig. 7a, b that $U \ll D$ and $I \ll F$, respectively, i.e., the SW radiation is dominated by downward fluxes while the LW radiation is dominated by upward fluxes. Figure 7c, d shows the pronounced tropopause at about 150 hPa.

The critical SB energy $Q^{(c)}$, along with the reference value $\vec{Q}$ (step 3), is shown in Fig. 8. Above the tropopause, Q is much higher than $Q^{(c)}$, owing to the high LW transmissivity t, i.e., small extinction coefficient $(1 - t)$ there. As one descends below the tropopause, Q approaches $Q^{(c)}$. This suggests a possible downward forking of the LW transmissivity profile t in the upper troposphere. In fact, the reference profile of LW transmissivity crosses the critical profile $t^{(c)}$ between layers 8 and 7, as shown in Fig. 8b (step 4). A bifurcated solution branch $t^{(b)}$ exists therefore below layer 7, as plotted in Fig. 8b (step 5). Because $t^{(b)}$ remains higher than $t^{(c)}$, this is the dry branch. The reference profile, on the other hand, is identical with the moist branch below layer 7. This is consistent with the fact that the reference profile was obtained from the ECMWF reanalysis over warm waters.

Figure 8c gives the relative humidity profiles corresponding to the two branches of t. The difference between the two humidity profiles, dry and moist, below 400 hPa is even more striking than for the LW transmissivities in Fig. 8b. Comparison of Fig. 8b and 8c with Fig. 4c and 4d shows our analytical bimodality results in Sect. 3.2 to be qualitatively consistent with the observed characteristics of the tropical atmosphere.

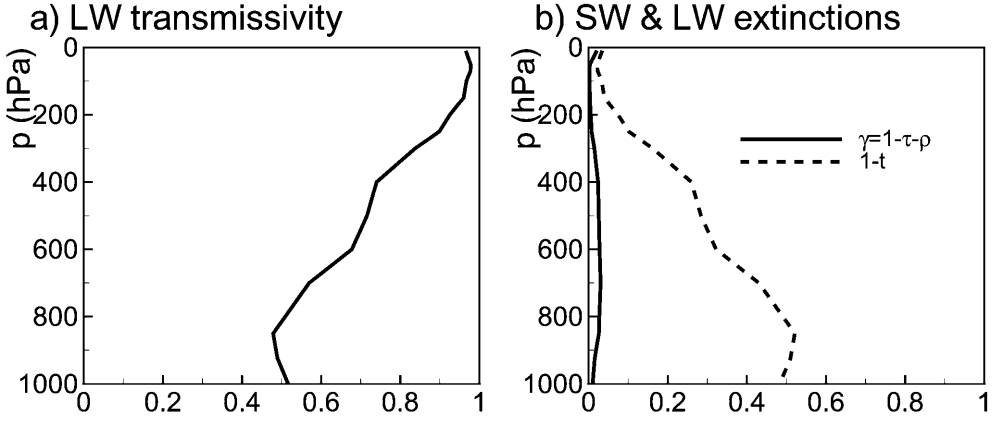

Fig. 6a, b SW and LW optical properties: **a** LW transmissivity $\vec{t}$; and **b** SW and LW extinction coefficients $\vec{\gamma} = (1 - \vec{\tau} - \vec{\rho})$ and $(1 - \vec{t})$

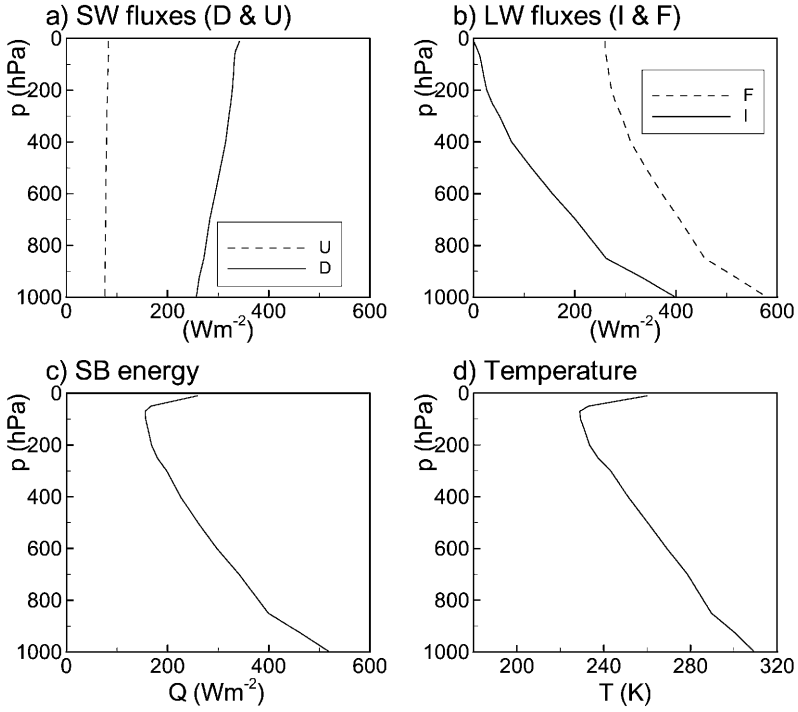

Fig. 7a–d Vertical profiles of **a** SW down- and upward flux $(\vec{D}, \vec{U})$; **b** LW down- and upward flux $(\vec{I}, \vec{F})$; **c** SB energy $\vec{Q}$; and **d** temperature $\vec{T}$

The critical LW transmissivity profile $t^{(c)}$ is mainly controlled by the SW extinction coefficient $\vec{\gamma}$. In the upper troposphere, where the observed atmosphere has very little humidity h, the LW transmissivity t always corresponds to the dry solution $t^{(d)}$. As the altitude drops below the tropopause, h increases and hence t tends to decrease. The SW extinction coefficient is rather small at this altitude and thus the nonlinear local conversion of energy E is suppressed. Hence t first satisfies the bifurcation condition in layer $i_*^{(c)}$ just above the mid-troposphere. Once the critical layer $i_*^{(c)}$ has been obtained, the LW transmissivity profile below it can lie either along the moist branch $t^{(m)}$ or the dry branch $t^{(d)}$, depending on the available water vapor and temperature in the lower troposphere.

The difference in transmissivity values t between the two branches in the lower troposphere is larger in the model than in the observations. This may be due to any one of the many simplifying hypotheses made in formulating our single-column model. Of these, the atmosphere's being in perfect radiative equilibrium is the most likely to lead to the discrepancy.

Finally the sensitivities $\partial Q_i/\partial t_j$ along the reference branch t and the bifurcated branch $t^{(b)}$ are computed to assess their stability (step 6), and the results are summarized in Table 4. Shine and Sinha (1991) have shown, using a 20-layer version of Manabe and Wetherald's (1967) radiative-convective model, that the model temperatures' sensitivity to changes in either absolute or relative humidity in each 50-hPa layer, and hence to layer-by-layer changes in LW transmissivity, behaves quite linearly. It follows that our analytically computed linear sensitivities should provide some guidance for more detailed and complex models as well.

Each column of Table 4 corresponds to the layer j where the LW transmissivity may change. As discussed in Sect. 2.3 and Appendix B, t_j influences the layers above $(j < i \leq n)$, the layer itself $(i = j)$, and those below $(0 \leq i < j)$ differently. The three entries in each column indicate the sensitivity $\partial Q_i/\partial t_j$ for these three parts of the atmosphere with respect to the layer j. The upper and lower panels of Table 4 contain the sensitivity along the reference and bifurcated branches, respectively.

The top entry of the column in both panels represents the sensitivity of the SB energy in the layers above the diagonal $(j < i \leq n)$, when changing the LW transmissivity of a given layer j: all these entries are identically zero. A change of t_j in a given layer has therefore no impact whatsoever on the SB energy, and therefore the temperature, profile above (see also Li et al. 1997).

The middle entry in each column represents the local sensitivity within the layer itself (see also Sect. 3.3). Along the reference profile, the sensitivity changes from positive to negative between layers 8 and 7, due to the switch from dry conditions in the stratosphere and upper troposphere to moist conditions in the middle and lower troposphere. The reference profile in our radiative-equilibrium model may thus be unstable in the lower troposphere due to the model's version of the "runaway greenhouse" effect. The bifurcated $t^{(b)}$ solution, on the contrary, is dry from top to bottom, has positive sensitivity throughout for $i = j$, and is therefore stable at all levels (see discussion in Sect. 3.3).

The bottom entry in each column is the sensitivity of Q_i to a change of t_j in all the layers between the surface and layer j $(0 \leq i < j)$. All entries are negative regardless of branch type, because a higher t_j value reduces the downward LW flux I_i that reaches layer i

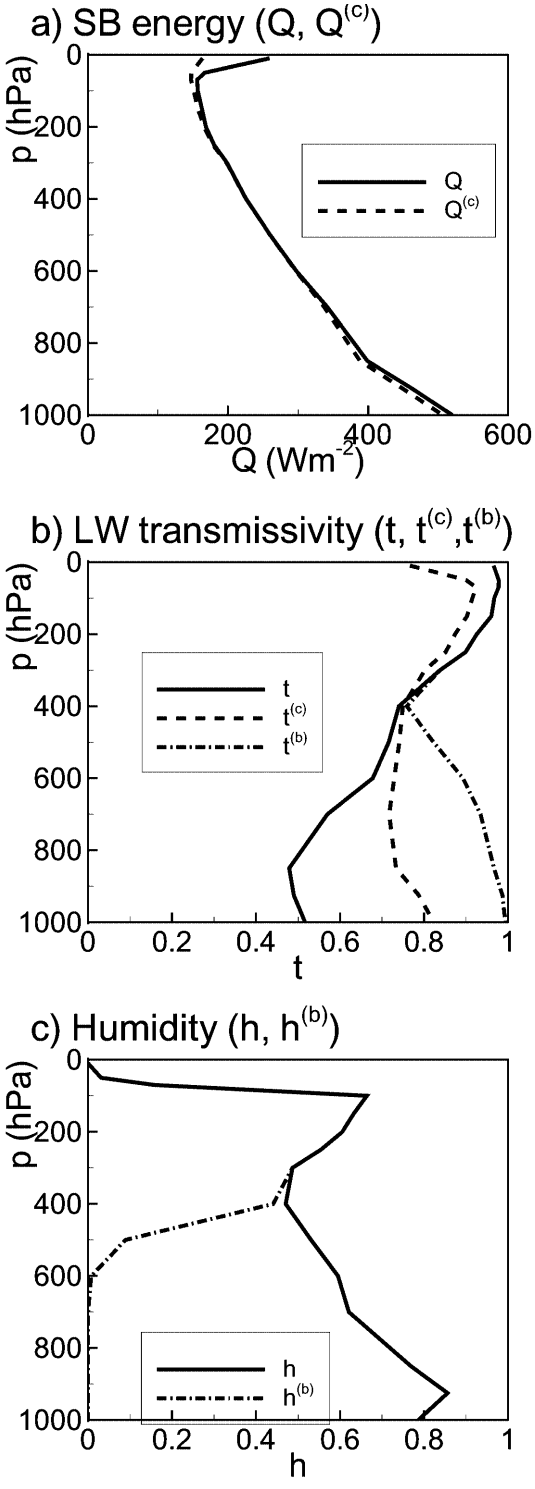

Fig. 8a–c Vertical profiles for multiple solutions: **a** SB energy – reference profile $\vec{Q}$ and critical profile $\vec{Q}^{(c)}$; **b** LW transmissivity – reference profile $\vec{t}$, critical profile $\vec{t}^{(c)}$, and forked profile $\vec{t}^{(b)}$; and **c** humidity – reference profile h and forked profile $h^{(b)}$

by letting the SB energy Q_j in the layer emit less (see Appendix B). If t increases in a given atmospheric layer for some reason, it leads to cooling of the atmosphere below (see also our discussion in Sect. 1.2). The sensitivity value $\partial Q_i/\partial t_j$, is in fact, the same for all layers i below j $(0 \le i < j)$. This means that, in our purely radiative model, introducing as it were an additional thickness of glass to the atmospheric greenhouse's "roof" (i.e., to a given layer j in the model atmosphere), will increase the SB energy Q_i in all layers $i < j$ below that roof by the same amount.

5 Concluding remarks

5.1 Summary

We used a highly idealized single-column model to investigate the fundamental characteristics of atmospheric temperature and optical properties in radiative equilibrium. Our main motivation in doing so was to understand the radiative effects that contribute to the observed spatial *homogeneity* of temperature profiles and *bimodality* of humidity and longwave transmissivity profiles. A number of simplifying assumptions were made in order to obtain a model that is transparent enough to solve analytically. We summarize here our results and discuss next their climatic implications, as well as their limitations.

Our model uses n layers $(1 \le i \le n)$ to discretize shortwave (SW) and longwave (LW) radiation in the vertical. Each of these consists of two-stream, up- and downward, fluxes (Figs. 1 and 2). The system is assumed to be in radiative equilibrium in the present model version, i.e., both convective mechanisms and exchanges of mass or heat with the ground or ocean below, $i = 0$, and adjacent columns are neglected. The thermal state of the atmosphere is fully described by its temperature profile $\vec{T} = (T_0, T_1, \ldots, T_n)^{\mathrm{T}}$ and associated Stefan-Boltzmann (SB) energy profile $Q_i = \sigma T_i^4$.

We use $n = 11$ model layers when obtaining its optical properties from the LMD GCM's vertical fluxes and $n = 15$ layers when applying our model to ECMWF's reanalysis results. This vertical resolution is comparable to the 17 layers of Hu and Randall's (1994) Model 1 and nine levels of their Model 2.

By solving the model analytically, we first examined the fundamental SW and LW radiative-transfer processes separately. The SW fluxes can be expressed as a function of the solar insolation S at the top-of-the-atmosphere and the SW optical properties, transmissivity $\vec{\tau}$ and reflectivity $\vec{\rho}$, only. The LW fluxes depend on the LW optical properties and the SB energy $\vec{Q}$. The extinction coefficients $\gamma_i = 1 - \tau_i - \rho_i$ were found to be key parameters in determining both SW and LW radiative processes.

A unique temperature profile and, therewith, SB energy profile is determined by radiative equilibrium between the SW and LW fluxes. SW radiation deposits a net SW flux in each layer; the latter is then redistributed by LW radiation throughout the atmosphere.

The SB energy in each layer is therefore expressed as a function of a given set of SW and LW optical

Table 4 Sensitivity $\partial Q_i/\partial t_j$ along the reference profile t_j (upper panel) and bifurcated profile $t_j^{(b)}$ (lower panel). Each column corresponds to layer j where t changes, while the three rows correspond to the atmospheric layers where the sensitivity $\partial Q_i/\partial t_j$ is computed: above ($j < i \leq n$), in the same layer ($i = j$), and below ($0 \leq i < j$). The sensitivities are identical in our model for all the layers above ($j < i \leq n$) and all the layers below ($0 \leq i < j$) layer j

Layer i of Q_i	Layer j of t_j														
	15	14	13	12	11	10	9	8	7	6	5	4	3	2	1
$i > j$	–	0	0	0	0	0	0	0	0	0	0	0	0	0	0
$i = j$	3686	1345	711	386	344	135	86	39	−6	−15	−25	−52	−71	−73	−71
$i < j$	−67	−64	−64	−64	−65	−67	−68	−71	−78	−77	−77	−84	−89	−84	−79
	Layer j of $t_j^{(b)}$														
$i > j$	(Same as upper panel)								0	0	0	0	0	0	0
$i = j$	(Same as upper panel)								5	69	282	722	1960	7192	19570
$i < j$	(Same as upper panel)								−76	−68	−60	−55	−50	−47	−46

properties. Furthermore, the contributions from all the layers below to the SB equilibrium in each layer enter only through their sum as total LW flux. Hence the detailed temperature profile of the atmosphere below a given layer does not matter in determining the temperature of that layer. The three main factors responsible for the SB energy, and hence temperature, profiles are: the SW extinction that determines the energy available to each layer; the local conversion and upward propagation of the energy so absorbed as LW fluxes; and the LW extinction that determines the efficiency of the local energy conversion.

With these analytical results on SW and LW fluxes in hand, we investigated the contribution of purely radiative processes to the homogeneity of temperatures and bimodality of humidities observed to exist in Earth's atmosphere at low latitudes. For this purpose, we first examined the observed profiles of temperature, humidity and optical properties using the ECMWF reanalysis for three areas, one for moist and two for dry air masses (see Figs. 3 and 4).

Spatial homogeneity in temperature is clearly observed in the ECMWF reanalysis throughout the tropics and subtropics, as expected. Bimodality, on the contrary, is found in LW transmissivity as well as in humidity profiles. The two main characteristics of this observed bimodality in both LW transmissivity and humidity are that (1) the two profiles are quite similar above and just below the tropopause, while (2) the dry-region and moist-region profile diverge as one descends into the lower troposphere. Moreover, a near-tropopause minimum of the SW extinction coefficient profile occurs consistently in all three regions.

Given these observations, we proceeded to find an explanation for them in terms of purely radiative processes. A unique feature that plays a major role in this explanation is the way we model the net SW flux absorbed in each layer. The net SW flux E_i is controlled by the extinction coefficient γ_i (see Eqs. 1 and 7). The nonlinear dependence of the SB energy on LW transmissivity is predicated, in turn, on the presense of E_i (see Eq. 16a).

This quadratic nonlinearity was derived analytically and it leads to the existence of two solution branches for the LW transmissivity, given prescribed insolation, surface and SW optical properties (see Fig. 5). We interpret the lower and higher LW transmissivity as our model's version of moist and dry conditions, and therefore high and low opacities, respectively. This interpretation is based on our observational study that used the ECMWF reanalysis.

The quadratic dependence of SB energy Q_i on LW transmissivity t_i (see Eq. 16) yields two solutions for t_i, one, or none, depending on whether Q_i exceeds a critical value $Q^{(c)}$, equals it, or falls short. The critical value $Q^{(c)}$ corresponds to the minimal temperature that is consistent with radiative equilibrium. We showed that LW transmissivity in the stratosphere corresponds to a dry profile, with $t = t^{(d)} \geq t^{(c)}$, and that equality of t with the critical $t^{(c)}$ occurs just below the tropopause.

Our reference profile of LW transmissivities is derived from the ECMWF reanalysis (see Fig. 4d). In our model's phase-parameter space, the quadratic nonlinearity mentioned above leads to *bifurcation* from this profile. In the model atmosphere's physical space, this bifurcation takes the form of a downward forking of the two distinct profiles, moist and dry (see Fig. 8). Above the critical level the unique profile is the dry one and it agrees with the observed reference values. Below this level where $t = t^{(c)}$, the two profiles diverge throughout the middle and lower troposphere, $t^{(m)} < t^{(c)} < t^{(d)}$.

The two conditions that favor bifurcation are: (1) a relatively small net SW flux, i.e., small extinction coefficient, and (2) moderately low LW transmissivity, i.e., nonnegligible humidity. Therefore the upper troposphere is ideally located to be the upper limit of the bimodality in LW transmissivities observed in the ECMWF reanalysis. Our analytical results are also consistent with this bimodality being less observable at higher latitudes, where dry profiles prevail on average in the observations.

The moist branch was shown to be unstable due to our model's version of the "runaway greenhouse" effect, while the dry branch is stable (see Table 4). This result is at least partially consistent with that of Rennó (1997), who found two stable equilibria in a radiative-convective model. His model allows for an explicit dependence of

humidity on temperature and other model quantities. One of his equilibria corresponds to an optically thick, the other to an optically thin atmosphere. Our results also agree in spirit with Pierrehumbert's (1995) distinction between the moist *furnace* and dry *radiator fins* that make up Earth's low-latitude atmosphere.

5.2 Discussion

A number of recent studies suggest that simple, single-column radiative-convective systems possess multiple regimes. Li et al. (1997) found that the surface albedo's nonlinear temperature dependence leads to three equilibria. These correspond roughly to the three climates, two stable and one unstable, found in energy-balance models (North et al. 1981; Ghil and Childress 1987).

Rennó (1997) also found two stable equilibria in his one-dimensional radiative-convective model, along with an unstable equilibrium that separates the two stable ones. In his work, the multiplicity of equilibria arises from nonlinearities in the model's hydrological cycle. More precisely, it is due to nonlinear feedbacks between the additional opacity introduced by water vapor, the radiative fluxes, and moist convection. Rennó's (1997) multiple equilibria correspond, essentially, to a nonlinearly saturated version of the "runaway greenhouse" instability. This instability of a unique equilibrium was originally found in earlier models (Komabayasi 1967; Ingersoll 1969; Nakajima et al. 1992), in which the temperature and optical thickness both increased, along with water-vapor concentration. The multiple equilibria of both Li et al. (1997) and Rennó (1997) thus involve distinct temperature profiles, along with distinct optical properties.

Our model's bimodality is different from Li et al.'s (1997) or Rennó's (1997). Ours arises from distinct LW transmissivity profiles for a given set of temperature profile, surface emissivity and SW optical properties. The basic mechanism here involves purely radiative processes that maintain the prescribed balance in the SB energy profile. The present model still mimics the "runaway greenhouse" instability of the "moist" profile of low LW transmissivities, while the "dry" profile is stable. The analytical results of our highly idealized single-column model are thus compatible with Pierrehumbert's (1995) interpretation of bimodality in low-latitude moisture profiles and their respective stabilities, even in the absence of temperature-humidity feedbacks.

The strength of our model lies in its exhaustive explanation of purely radiative processes, its weakness in its limitation to such processes. By omitting convective processes, our model could be solved analytically downward from the top of the atmosphere to the surface. This provides a self-consistent reason for bimodality to exist only below the tropopause.

The main cause of humidity, and hence optical thickness, increase in Earth's atmosphere, however, is convection from the surface and planetary boundary layer. Adding upward convective processes may lead to an imbalance in our model atmosphere. Such an imbalance could result from possible inequalities between the downward radiative fluxes in the present model and the combined upward fluxes of sensible and latent heat in the modified model. This imbalance may give rise to oscillations in the model's atmosphere, such as the quasi-stationary, convective component of the Madden-Julian (1971) oscillation addressed by the work of Hu and Randall (1994). The extent to which the oscillation obtained by these authors depends, for its existence and its period, on the heat capacity and air-sea fluxes of the ocean mixed layer deserves further investigation, as does its interaction with dynamical processes in the observed oscillation (Emanuel et al. 1994; Neelin and Yu 1994).

Another interesting problem that can be explored by using a somewhat more complete, but still simple model is that of how radiative, or radiative-convective, equilibria within two adjacent areas, moist and dry, might affect each other. Such an exploration would be of interest even in the absence of dynamics or allowing only for very highly simplified dynamics. A two-column model of this type would represent a further step in a hierarchy of radiative-convective models beyond the two-box model of Pierrehumbert (1995) and the single-column models of Hu and Randall (1994), Rennó (1997), and the present authors. The two areas modeled may be separated in latitude, like the tropics and subtropics (Hartman et al. 1986), or in longitude, like the western and eastern tropical Pacific or like the wet Amazon Basin (Zeng and Neelin 1999) and the dry Nordeste of Brazil.

The simplest version of a model constructed to address this problem would consider the radiative equilibrium of the two columns representing the moist and dry regions that exchange energy with each other layer by layer. By increasing the degree of realism of our model step by step in various directions, we hope to deepen our understanding of radiative and convective processes and their role in maintaining as well as modifying observed climate behavior.

Acknowledgements The authors would like to acknowledge stimulating discussions with Drs. Rong Fu, Hervé Grenier, Raymond T. Pierrehumbert, and Nilton Rennó. MG would like to thank his hosts at the Laboratoire de Météorologie Dynamique du CNRS and the Ecole Normale Supérieure in Paris for their hospitality during the sabbatical that helped complete this work. Our work was supported by the United States' National Aeronautics and Space Administration Grant NAG 5-9294 (KI), a National Science Foundation Special Creativity Award (MG), as well as by French and European grants (HLT and ZXL). This is publication number 5484 of UCLA's Institute of Geophysics and Planetary Physics.

Appendix A Solutions for the radiative-transfer equations

Owing to the linearity of the SW and LW fluxes in the transfer relations given by Eqs. (6) and (8), our radiative-equilibrium model can be solved in full, either recursively or by matrix operations.

A.1 Shortwave stream

A.1.1 Recursive formulae

Using the recursive formula of Eq. (6b), the upward SW flux U_i can be expressed in terms of downward flux D_l and SW optical properties (τ_l, ρ_l) with $l \leq i$

$$U_i = \sum_{l=0}^{i} \left(\prod_{m=l+1}^{i \geq l+1} \tau_m \right) \rho_l D_l \ ; \tag{A.1}$$

here $\rho_l D_l$ corresponds to the flux that has changed its direction of propagation from down- to upward at level l by reflection. The product:

$$\prod_{m=l+1}^{i \geq l+1} \tau_m \equiv \begin{cases} \tau_{l+1}\tau_{l+2}\cdots\tau_i, & \text{for } i \geq l+1, \\ 1, & \text{otherwise} \end{cases} \tag{A.2}$$

evaluates the flux that has propagated directly through the layers between $l+1$ and i without any reflection. Therefore U_i is a collection of the downward fluxes that have reached and been reflected from all levels below i and have then propagated upward to reach level i, without any further reflection.

In order to solve Eq. (6c) for the downward flux D_i subject to U_j given by Eq. (A.1), we define direct downward flux $\bar{D}_i$ and its normalization $\bar{d}_i$ as follows:

$$\bar{D}_i \equiv D_i \left(\prod_{m=0}^{i \geq 0} \tau_m \right) \equiv \bar{D}_0 \bar{d}_i \ , \tag{A.3a}$$

with initial condition:

$$\bar{d}_0 = 1 \ . \tag{A.3b}$$

Here $\bar{D}_0$ is a normalization constant yet to be determined; $\bar{D}_i$ is that part of downward D_i, for $1 \leq i \leq n$, that propagates from level i downward to reach level 0 without any reflection. Using Eqs. (A.3a) and (6c), we obtain a recursive equation for $\bar{d}_i$:

$$\bar{d}_i = \bar{d}_{i-1} - \sum_{l=0}^{i-1} \rho_i \rho_l \left(\prod_{m=l+1}^{i-1 \geq l+1} \tau_m \right)^2 \bar{d}_l \ , \tag{A.4}$$

which can be solved upward from $i = 0$ with the initial condition Eq. (A.3b). The constant $\bar{D}_0$ is then obtained by matching the boundary condition at the top-of-the-atmosphere:

$$\bar{D}_n = \bar{D}_0 \bar{d}_n = \frac{S}{4} \left(\prod_{m=0}^{n \geq 0} \tau_m \right) \ . \tag{A.5}$$

Consequently the analytical form of the SW fluxes is given by:

$$(\vec{D}, \vec{U}) = \frac{S}{4} (\vec{d}, \vec{u}) \ , \tag{A.6a}$$

where

$$\begin{aligned} d_i(\vec{\tau}, \vec{\rho}; \rho_0) &= \frac{\left(\prod_{m=0}^{n \geq 0} \tau_m \right)}{\bar{d}_n} \bar{d}_i; \\ u_i(\vec{\tau}, \vec{\rho}; \rho_0) &= \sum_{l=0}^{i} \bar{d}_l \rho_l \left(\prod_{m=l+1}^{i \geq l+1} \tau_m \right) \ . \end{aligned} \tag{A.6b}$$

A.1.2 Matrix formulae

While the recursive formulae provide the explicit expression of the exact solutions, matrix formulae give an alternate, systematic approach to solving the radiative-transfer equations.

The transfer relation for $\vec{U}$ given by Eq. (6b) can be written as a homogeneous vector equation:

$$\vec{U} = \mathbf{R}^{(\mathrm{D})} \vec{D} + \mathbf{T}^{(\mathrm{U})} \vec{U} = \tilde{\mathbf{T}}^{(\mathrm{U})} \mathbf{R}^{(\mathrm{D})} \vec{D} \ , \tag{A.7a}$$

where:

$$R_{ij}^{(\mathrm{D})} = \begin{cases} \rho_i, & \text{for } i = j, \\ 0, & \text{otherwise;} \end{cases} \quad T_i^{(\mathrm{U})} = \begin{cases} \tau_i, & \text{for } i = j-1, \\ 0, & \text{otherwise} \ . \end{cases} \tag{A.7b}$$

Here $\mathbf{R}$ and $\mathbf{T}$ denote the reflective and transmissive $(n+1) \times (n+1)$-dimensional matrix operators, respectively, and the superscripts $\{\cdot\}^{(D)}$ and $\{\cdot\}^{(U)}$ relate to the flux on which they act. Note that $\mathbf{R}^{(\mathrm{D})}$ is a diagonal matrix, while $\mathbf{T}^{(\mathrm{U})}$ has only its main subdiagonal nonzero. Furthermore:

$$\tilde{T}_{ij}^{(\mathrm{U})} \equiv (\mathbf{Id} - \mathbf{T}^{(\mathrm{U})})^{-1}|_{ij} = \begin{cases} \left(\prod_{m=i+1}^{j \geq i+1} \tau_m \right) & \text{for } i \geq j, \\ 0, & \text{otherwise} \ , \end{cases} \tag{A.8}$$

is an $(n+1) \times (n+1)$-dimensional matrix operator associated with direct transmission, while **Id** stands for the $(n+1) \times (n+1)$-dimensional identity matrix. The upper triangular structure of $\tilde{\mathbf{T}}^{(\mathrm{U})}$ shows that U_i receives the contribution from the direct propagation of the reflected D_j only from below (i.e., for $j \leq i$), but not from above, as discussed for the recursive formulae in the preceding subsection.

Similarly, the transfer relation for downward flux $\vec{D}$ given by Eq. (6c) can be written as an inhomogeneous vector equation due to the boundary condition at the top-of-the-atmosphere:

$$\vec{D} = \mathbf{T}^{(\mathrm{D})} \vec{D} + \mathbf{R}^{(\mathrm{U})} \vec{U} + \frac{S}{4} \vec{B} = \tilde{\mathbf{T}}^{(\mathrm{D})} (\mathbf{R}^{(\mathrm{U})} \vec{U} + \frac{S}{4} \vec{B}) \ , \tag{A.9}$$

where

$$\begin{aligned} T_{ij}^{(\mathrm{D})} &= \begin{cases} \tau_i, & \text{for } i = j+1, \\ 0, & \text{otherwise;} \end{cases} \quad R_{ij}^{(\mathrm{U})} = \begin{cases} \rho_{j-1}, & \text{for } i = j, \\ 0, & \text{otherwise;} \end{cases} \\ \vec{B}_i &= \begin{cases} 1, & \text{for } i = n, \\ 0, & \text{otherwise} \ ; \end{cases} \end{aligned} \tag{A.10}$$

and

$$\tilde{T}_{ij}^{(\mathrm{D})} \equiv (\mathbf{Id} - \mathbf{T}^{(\mathrm{D})})^{-1}|_{ij} = \begin{cases} \left(\prod_{m=j+1}^{i \geq j+1} \tau_m \right) & \text{for } i \geq j, \\ 0, & \text{otherwise} \ . \end{cases} \tag{A.11}$$

Equations (A.7a) and (A.9) can be combined to express the balance between $\vec{D}$ and solar forcing:

$$(\mathbf{Id} - \tilde{\mathbf{T}}^{(\mathrm{D})} \mathbf{R}^{(\mathrm{U})} \tilde{\mathbf{T}}^{(\mathrm{U})} \mathbf{R}^{(\mathrm{D})}) \vec{D} = \tilde{\mathbf{T}}^{(\mathrm{D})} \frac{S}{4} \vec{B} \ . \tag{A.12}$$

The left-hand side indicates that the downward flux has two components: one pure (**Id**) and the other twice-reflected $(\tilde{\mathbf{T}}^{(\mathrm{D})} \mathbf{R}^{(\mathrm{U})} \tilde{\mathbf{T}}^{(\mathrm{U})} \mathbf{R}^{(\mathrm{D})})$. The right-hand side (RHS) is the direct downward propagation of the solar forcing from the top. By solving this balance equation for $\vec{D}$ and substituting the solution into Eq. (A.7a), we obtain:

$$(\vec{U}, \vec{D}) = (\tilde{\mathbf{T}}^{(\mathrm{U})} \mathbf{R}^{(\mathrm{D})}, \ \mathbf{Id}) \ (\mathbf{Id} - \tilde{\mathbf{T}}^{(\mathrm{D})} \mathbf{R}^{(\mathrm{U})} \tilde{\mathbf{T}}^{(\mathrm{U})} \mathbf{R}^{(\mathrm{D})})^{-1} \tilde{\mathbf{T}}^{(\mathrm{D})} \frac{S}{4} \vec{B} \ . \tag{A.13}$$

The SW stream is thus expressed in its entirety as a combined, down- and upward, flux induced by the solar forcing imposed at the top of the atmosphere.

A.1.3 Second-order solution

Li et al. (1997) obtained the solution for the SW fluxes as a first-order approximation by neglecting terms that are equal to or higher than the second order in ρ_i for all i, $0 \leq i \leq n$. Their approximation neglects the second-order term in surface albedo ρ_0 as well. Since ρ_0 is considerably larger than the atmospheric SW reflectivity ρ_i for $1 \leq i \leq n$, it appears desirable to treat ρ_0 separately from ρ_i.

We keep therefore terms up to the second order in ρ_0, while still neglecting the second- and higher-order terms in ρ_i for $1 \leq i \leq n$ when solving the recursive relation given by Eq. (A.4). This yields a new, second-order accurate solution:

$$(\vec{D}, \vec{U}) = \frac{S}{4} (\vec{d}', \vec{u}') + \frac{S}{4} \{ \mathcal{O}(\rho_l^2), \mathcal{O}(\rho_0 \rho_l^2) \} \ , \tag{A.14}$$

where $1 \le l \le n$. The prime denotes this second-order solution, which is "halfway" in accuracy between Li et al.'s (1997) and the one used throughout the rest of this work:

$$d_i'(\vec{\tau},\vec{\rho},\rho_0) = (\prod_{m=i+1}^{n\ge i+1}\tau_m)\{1+\rho_0\sum_{l=i+1}^{n}\rho_l(\prod_{m=i+1}^{l-1\ge i+1}\tau_m)^2\} = d_i^{(01)} + d_i^{(11)} \ ; \tag{A.15a}$$

and

$$u_i'(\vec{\tau},\vec{\rho},\rho_0) = \rho_0(\prod_{m=1}^{i\ge 1}\tau_m)(\prod_{m=1}^{n\ge 1}\tau_m) + \sum_{l=1}^{i}\rho_l(\prod_{m=l+1}^{i\ge l+1}\tau_m)(\prod_{m=l+1}^{n\ge l+1}\tau_m) + \rho_0^2\sum_{l=0}^{i}\rho_l(\prod_{m=1}^{l-1\ge 1}\tau_m)(\prod_{m=1}^{n\ge 1}\tau_m)(\prod_{m=1}^{i\ge 1}\tau_m) = u_i^{(10)} + u_i^{(01)} + u_i^{(21)} \ . \tag{A.15b}$$

The pair of superscripts in parentheses refers to the number of reflections at the surface (first superscript) and upper-air level (second superscript), respectively. Figure A.1 shows the schematics of the solutions obtained by the new approximation, along with the order of each flux component.

The primary benefit of this higher-order approximation is to better illustrate the fundamental radiative processes that underly the exact SW-stream solution given by Eq. (A.6), without sacrificing the solution's accuracy. As shown in Fig. A.1, the downward flux $\vec{d}'$ consists of two principal components, $\vec{d}^{(00)}$ and $\vec{d}^{(11)}$. The upward flux $\vec{u}'$ has three such components, $\vec{u}^{(10)}$, $\vec{u}^{(01)}$, and $\vec{u}^{(21)}$. Note that all these components are measured at the top of the atmosphere, due to the boundary condition imposed there.

A.2 Longwave stream

An analytical expression of the exact solution for the LW fluxes can be obtained by solving the recursive relations given by Eq. (8). The up- and downward fluxes $(\vec{F},\vec{I})$ are expressed in terms of the optical properties $(\vec{t},\vec{r})$ and the SB flux $\vec{Q}$:

$$F_i = \sum_{l=0\le i}^{i\ge 0}\frac{1}{b_l}(1-t_l)(\prod_{m=l+1}^{i\ge l+1}t_m)Q_l; \qquad I_i = \sum_{l=i+1}^{n\le i}\frac{1}{b_l}(1-t_l)(\prod_{m=i+1}^{l-1\ge i+1}t_m)Q_l \ . \tag{A.16}$$

The upward LW flux F_i is therefore a collection of upward emissions Q_l from layer l below i ($l < i$); each such emission propagates upward through the layers $l+1$ to i without reflection. The downward counterpart of F_i from the layers above ($l > i$) is I_i.

The LW stream can be described by vector-matrix equations as well. The vectors $\vec{F}$ and $\vec{I}$ satisfy a set of inhomogeneous equations:

$$\vec{F} = \mathbf{T}^{(\mathrm{F})}\vec{F} + \mathbf{R}^{(\mathrm{F})}Q, \tag{A.17a}$$

$$\vec{I} = \mathbf{T}^{(\mathrm{I})}\vec{I} + \mathbf{R}^{(\mathrm{I})}\vec{Q} \ ; \tag{A.17b}$$

here

$$T_{ij}^{(\mathrm{F})} = \begin{cases} t_i, & \text{for } i+1=j,\\ 0, & \text{otherwise;}\end{cases} \quad T_{ij}^{(\mathrm{I})} = \begin{cases} t_i, & \text{for } i=j+1,\\ 0, & \text{otherwise;}\end{cases} \quad R_{ij}^{(\mathrm{F})} = \begin{cases} \frac{1}{b_i}(1-t_i), & \text{for } i=j,\\ 0, & \text{otherwise;}\end{cases} \quad R_{ij}^{(\mathrm{I})} = \begin{cases} \frac{1}{b_{j-1}}(1-t_{j-1}), & \text{for } n>i=j,\\ 0, & \text{otherwise} \ .\end{cases} \tag{A.17c}$$

Therefore

$$(\vec{F},\vec{I}) = (\tilde{\mathbf{T}}^{(\mathrm{F})}\mathbf{R}^{(\mathrm{F})},\tilde{\mathbf{T}}^{(\mathrm{I})}\mathbf{R}^{(\mathrm{I})})\ \vec{Q} \ , \tag{A.18a}$$

where

$$\tilde{T}_{ij}^{(\mathrm{F})} \equiv (\mathbf{Id}-\mathbf{T}^{(\mathrm{F})})^{-1}|_{ij} = \begin{cases} (\prod_{m=i+1}^{j\ge i+1}t_m) & \text{for } i\le j,\\ 0, & \text{otherwise;}\end{cases} \quad \tilde{T}_{ij}^{(\mathrm{I})} \equiv (\mathbf{Id}-\mathbf{T}^{(\mathrm{I})})^{-1}|_{ij} = \begin{cases} (\prod_{m=j+1}^{i\ge j+1}t_m) & \text{for } i\ge j,\\ 0, & \text{otherwise} \ .\end{cases} \tag{A.18b}$$

The LW stream is thus induced by the SB energy emission in each layer.

A.3 Stefan-Boltzmann energy

The analytical form of the energy redistribution matrix $\mathbf{L} = \mathbf{L}(\vec{t},\vec{r})$ in Eq. (15b) allows us to state a few remarkable properties of the redistribution process of SW radiation by the LW stream. Here are the most important ones.

1. Provided $b_i = b_j$ (see Sect. 3.1 for justification), the redistribution is symmetric, $L_{ij} = L_{ji}$. That is, the ratio of the two contributions, from E_i to Q_j and from E_j to Q_i, is equal to one.
2. The matrix $\mathbf{L}$ is diagonally dominant, i.e., the diagonal entry L_{ii} is always larger than all the off-diagonal entries in the same row or column, $L_{ii} > L_{ij}$, $j \ne i$. This means that the redistribution effect is the strongest within the layer itself, due to the $1/(1-t_i^2)$ term. As t_i approaches one while keeping b_i constant, L_{ii} and hence Q_i must go up rapidly.
3. For fixed i, let us consider how L_{ij} changes as j varies from the top ($j = n$) to the surface ($j = 0$), i.e., how much each E_j contributes to Q_i. As j approaches i from above, L_{ij} increases by the additive term $(1-t_j)/(1+t_j)$; it achieves its maximum due to the $1/(1-t_i)$ term at $j = i$, and then remains uniform below i. Thus the contribution from the layers above ($j > i$) is more effective, the closer j is to i. The efficiency is maximum at $j = i$:

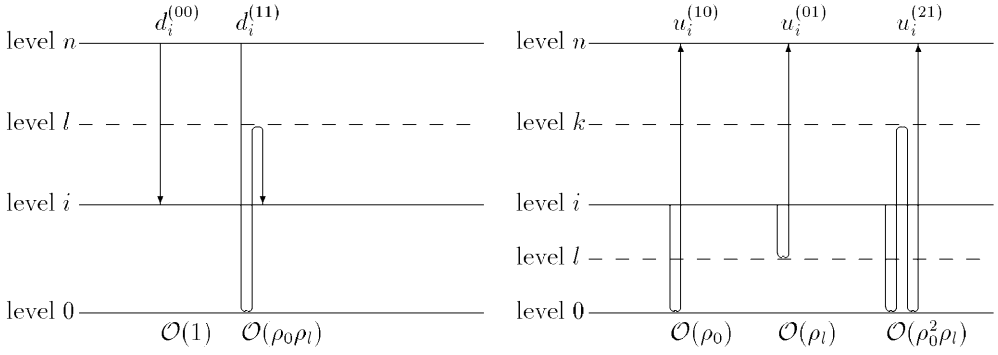

Fig. A.1 Schematics of the second-order solution for SW fluxes

the most significant contribution comes locally from the layer itself. The contribution to Q_i is uniform from the layers below ($j < i$). The last fact can also be seen in the first term of the RHS in Eq. (10a): the contribution to Q_i from the layers below takes the form of the total flux W_{i-1}; the vertical structure of the individual fluxes W_j or H_j in the layers below ($j < i$) does not influence Q_i.

4. For fixed j, let us consider how L_{ij} changes as i varies from the top ($i = n$) to the surface ($i = 0$), i.e., how much E_j contributes to each Q_i. As i approaches j from above, L_{ij} increases by the additive term $(1 - t_i)/(1 + t_i)$; it achieves its maximum due to the $1/(1 - t_i)$ term at $i = j$, then remains constant below j. This means that E_j's upward contribution to Q_i decreases as i goes up; E_j is most efficiently converted to Q_i within the same layer, at $i = j$. Any layer i lower than j ($i < j$) receives an equal contribution from E_j.
5. L_{ij} does not depend on LW transmissivity t_j for $j < i$, that is, the lower layers act in bulk and the details of their vertical profile do not matter to the SW flux of the layers above; see also item (3).

B Sensitivity of the Stefan-Boltzmann energy

The sensitivity of Q_i with respect to t_j can be obtained by differentiating Eq. (15b) directly or considering the simplified form of Eq. (16):

$$\frac{\partial Q_i}{\partial t_j} = \begin{cases} 0, & \text{for } i > j; \\ \frac{1}{b_i}\left\{\frac{-1}{(1+t_i)^2}A_{i-1} + \frac{2t_i}{(1-t_i^2)^2}E_i\right\} + \left[(b_i Q_i - I_i)\frac{\partial}{\partial t_i}\left(\frac{1}{b_i}\right)\right], & \text{for } i = j; \\ \frac{1}{b_i}\frac{-E_j}{(1+t_j)^2}, & \text{for } i < j \quad . \end{cases} \tag{B.1}$$

The terms in square brackets are the effects of changes in the conversion coefficients b_i; we take them to equal zero because the coefficients are nearly constant and we assume $b_i \equiv 1$ for simplicity.

From Eq. (16a) for $i \neq j$, it follows that t_j may influence Q_i only by changing I_i, i.e., $\partial Q_i/\partial t_j = (1/b_i)\partial I_i/\partial t_j$. The downward LW flux I_i depends on the LW transmissivity t_j of the layers above ($i < j$), but not of the layers below ($i > j$). The sensitivity $\partial Q_i/\partial t_j$ is therefore identically zero for $i > j$. It is always negative for $i < j$ because an increase of t_j reduces the emission of Q_j, and therewith the LW downward flux I_i available to the layers below j. Within the layer itself ($i = j$), the sign of the sensitivity is determined by a nonlinear competition between contributions from the lower layers (A_{i-1} term) and the layer itself (E_i term). These simple qualitative deductions are illustrated by the numerical values of $\partial Q_i/\partial t_j$ that appear in Table 4.

The upper panel in the table shows that, for the reference profile, the sensitivity $\partial Q_i/\partial t_j$ of the SB energy in a given layer i increases in absolute value within the troposphere, as the perturbed layer j (with $i < j$) is lower, and by the same amount for all layers i below j. Along the bifurcated profile (lower panel), when the perturbed layer j lies below the critical layer $j_*^{(c)}$ where the bifurcation actually occurs, the sensitivity decreases in absolute value as the perturbed layer decreases in altitude.

The sensitivity results shown in Table 4 for this purely radiative model with prescribed SW optical properties correspond more closely to results in a radiative-convective model, like that of Manabe and Wetherald (1967) or Shine and Sinha (1991), when changing absolute humidity layer by layer. The maximum sensitivity of SB energies Q_i for a dry profile is then near the surface, while for a moist profile it is at about 400 hPa.

The sensitivity of the temperatures T_i, rather than SB energies Q_i, is easily obtained from

$$\frac{\partial Q_i}{\partial t_j} = 4\sigma T_i^3 \frac{\partial T_i}{\partial t_j} \quad . \tag{B.2}$$

In particular, we obtain for the layers i that lie below a perturbed layer j ($i < j$),

$$\frac{\partial T_i/\partial t_j}{\partial T_{i-1}/\partial t_j} = \left(\frac{T_{i-1}}{T_i}\right)^3 \quad , \tag{B.3}$$

since $\partial Q_i/\partial t_j = \partial Q_{i-1}/\partial t_j$. The proportionality in Eq. (B.3) can be verified column by column and for each row, in the upper panel of Table 2 in Li et al. (1997). The numerical agreement there is only approximate because of round-off errors that arise from the numerical matrix inversion used to compute $\partial Q_i/\partial t_j$ in their model, while here the system (15) was solved analytically.

Shine and Sinha (1991) emphasized, based on the observed seasonal cycle of water vapor in the atmosphere, as well as on detailed radiative-convective calculations derived from GCM simulations, that different sensitivities are obtained when perturbations of relative, rather than absolute humidity are considered. We compute, therefore, also the logarithmic derivatives

$$t_j \frac{\partial T_i}{\partial t_j} = \frac{t_j}{4\sigma T_i^3}\frac{\partial Q_i}{\partial t_j} = \frac{T_i}{4}\frac{t_j}{Q_i}\frac{\partial Q_i}{\partial t_j} \quad . \tag{B.4}$$

A sensitivity table for these perturbations in relative transmissivity, according to Eq. (B.4), has been computed, in the format of Table 2 in Li et al. (1997), for both the reference branch t and the dry, bifurcated branch $t^{(b)}$ (not shown). The computations here, as in Table 2 of Li et al. (1997) and in Table 4 herein, are all subject to the constraint of fixed S at the top-of-the-atmosphere and exact radiative equilibrium throughout the column.

On the reference branch, which is moist below the forking point ($i \leq 7$), the surface-air temperature T_1 depends in an unstable manner on t_j: all the derivatives $t_j(\partial T_i/\partial t_j)$ are negative; or the LW transmissivity has to decrease with the temperature (and humidity) and hence will increase temperature further. Furthermore, the sensitivities depend only very weakly on height.

In agreement with the results shown in Table 4, the difference between the sensitivities for the reference and bifurcated branches is restricted to lie below the forking point in the LW transmissivity profile, i.e., to $i \leq 7$. The only substantial differences occur along the diagonal $i = j$; here the sensitivities on the lower, moist portion of the reference branch are small and negative. The sensitivities on the dry, bifurcated branch are large and positive, indicating very strong stability. The sensitivities of the surface-air temperature T_1 to upper-air changes in LW transmissivity are negative, like those on the moist branch, and very close to them in numerical values.

C Latitude dependence of the bimodality

The bimodality's dependence on latitude comes into play through the boundary condition for SW fluxes at the top-of-the-atmosphere, i.e., through the solar insolation $\tilde{S} = S\cos\tilde{\varphi}$. Here $\tilde{\varphi}$ is the latitude and the tilde denotes any variable that depends on latitude. For a given set of SW optical properties $(\tau, \rho; \rho_0)$, the SW fluxes are scaled by $\cos\tilde{\varphi}$:

$$(\tilde{A}_i, \tilde{E}_i; \tilde{D}_i, \tilde{U}_i) = (A_i\cos\tilde{\varphi}, E_i\cos\tilde{\varphi}; D_i\cos\tilde{\varphi}, U_i\cos\tilde{\varphi}) \quad ; \tag{C.1}$$

in this equation $(A_i, E_i; D_i, U_i)$ are the fluxes at the Equator. We assume that temperatures are homogeneous throughout the low-latitude belt, and hence $\tilde{Q}_i \equiv Q_i$. The conversion coefficients are also assumed to be independent of latitude, i.e., $\tilde{b}_i \equiv b_i$.

Given these notations and assumptions, the local LW transmissivity $\tilde{t}$ and downward flux $\tilde{I}$ satisfy the following relation:

$$\begin{aligned} Q_i &= \frac{1}{b_i}\left\{\left(\frac{A_{i-1}}{1+\tilde{t}_i} + \frac{E_i}{1-\tilde{t}_i^2}\right)\cos\tilde{\varphi} + \tilde{I}_i\right\}, \quad \text{for } 1 \leq i \leq n; \\ Q_0 &= \frac{1}{\tilde{r}_0}\left\{\frac{A_0 + A_1}{1+\tilde{t}_1}\cos\tilde{\varphi} + \tilde{I}_1\right\} \quad . \end{aligned} \tag{C.2}$$

$$\tilde{t}_i = \begin{cases} \dfrac{1}{2(b_i Q_i - \tilde{I}_i)} \left\{ A_{i-1}\cos\tilde{\varphi} \pm \sqrt{b_i(Q_i - \tilde{Q}_i^{(c)})\{b_i(Q_i + \tilde{Q}_i^{(c)}) - 2\tilde{I}_i - A_i\cos\tilde{\varphi}\right\}} & \text{for } Q_i > \tilde{Q}_i^{(c)}; \\ \varepsilon_i + 1 - (\varepsilon_i^2 + 2\varepsilon_i)^{1/2} \equiv t_i^{(c)} & \text{for } Q_i = \tilde{Q}_i^{(c)} \ , \end{cases} \tag{C.3}$$

This leads to multiple equilibrium solutions for $\tilde{t}$:
where

$$\tilde{Q}_i^{(c)} = \frac{1}{b_i}\{\frac{1}{2}(A_i + \sqrt{A_i^2 - A_{i-1}^2})\cos\tilde{\varphi} + \tilde{I}_i\} \ . \tag{C.4}$$

Note that $\tilde{t}_i$ and $\tilde{Q}_i^{(c)}$ are $\tilde{\varphi}$-dependent while $t_i^{(c)}$ and Q_i are not. Therefore the effect of latitude $\tilde{\varphi}$ on the bimodality of LW transmissivity profiles can be examined by considering the behavior of $\tilde{t}_i$ with respect to t_i and $t_i^{(c)}$, or equivalently that of $\tilde{Q}_i^{(c)}$ with respect to Q_i and $Q_i^{(c)}$.

From Eq. (C.2) it follows that, in order to sustain the radiative equilibrium through sufficiently high values of Q, for a set of prescribed conditions $(A_{i-1}, E_i; Q_i; b_i, \tilde{\varphi})$, at least one of the following three circumstances must hold: (1) higher inflow of upward flux from below (A_{i-1} term), i.e., $\tilde{t}_i < t_i$ with $\tilde{t}_i$ on the moist branch; (2) efficient local conversion within the layer (E_i term), i.e., $\tilde{t}_i > t_i$ with $\tilde{t}_i$ on the dry branch; or (3) massive downward flux from above ($\tilde{I}_i$ term), i.e., $\tilde{t}_j < t_j$ with $\tilde{t}_j$ on the moist branch in the lower layers, due to $\partial I_i/\partial t_j < 0$ for any $i < j$ (see Appendix B).

To systematically examine the latitudinal dependence of bimodality for the entire vertical LW transmissivity profile, we start from the top of the atmosphere. In the top layer n, the critical SB energy is:

$$\begin{aligned} \tilde{Q}_n^{(c)} &= \frac{1}{2b_n}(A_n + \sqrt{A_n^2 - A_{n-1}^2})\cos\tilde{\varphi} \\ &= Q_n^{(c)}\cos\tilde{\varphi} \le Q_n^{(c)} < Q_n \ , \end{aligned} \tag{C.5}$$

and therefore the gap between $\tilde{Q}_n^{(c)}$ and Q_n increases with latitude. Moreover, it follows from the equilibrium condition for SB energy,

$$Q_n = \frac{1}{b_n}(\frac{A_{n-1}}{1+\tilde{t}_n} + \frac{E_n}{1-\tilde{t}_n{}^2})\cos\tilde{\varphi} \ , \tag{C.6}$$

that energy conversion within layer n (the E_n term) is more efficient at higher latitudes than at the Equator on the $t^{(d)}$ branch. This conversion leads, therefore, to the local LW transmissivity $\tilde{t}_n$ being higher than t_n, which in turn exceeds its critical value $t_n^{(c)}$, i.e., $\tilde{t}_n > t_n > t_n^{(c)}$.

A higher $\tilde{t}_n$ then reduces the emission of Q_n into the layer below, i.e., $\tilde{I}_{n-1} < I_{n-1}$. Consequently, the critical SB energy drops further in layer $n-1$, i.e., $\tilde{Q}_{n-1}^{(c)} < Q_{n-1}^{(c)} < Q_{n-1}$ according to Eq. (C.4); simultaneously the LW transmissivity must go up, i.e., $\tilde{t}_{n-1} > t_{n-1} > t_{n-1}^{(c)}$, for more efficient local energy conversion to sustain the radiative equilibrium for a prescribed Q_{n-1}.

These circumstances are inherited, layer by layer, downward along the reference branch, (which is dry at high altitudes) until bifurcation occurs in some layer i where enough $\tilde{I}_i$ has accumulated for $\tilde{Q}_i^{(c)}$ to reach Q_i or $\tilde{t}_i$ is low enough to reach $t_i^{(c)}$ due to high humidity. Such a condition will be satisfied at a moderate latitude, if it ever be satisfied, in a layer lower than at the Equator, $\tilde{i}_*^{(c)} < i_*^{(c)}$. Moreover, the dry reference branch is stable, as discussed in Sect. 3.3 This state of affairs may contribute, along with dynamical processes, to the fact that moist profiles are less observable, on average, at higher latitudes.

References

Bony SK, Lau KM, Sud YC (1997) Sea-surface temperature and large-scale circulation influences on tropical greenhouse effect and cloud radiative forcing. J Clim 10: 2055–2077

Cess RD, Zhang MH , Minis P, Corsetti L, Dutton EG, Forgan BW, Garber DP, Gates WL, Hack JJ, Harrison EF, Jing X, Kiehl JT, Long CN, Morcrette JJ, Potter GL, Ramanathan V, Subasilar B, Whitlock CH, Young DF, Zhou Y (1995) Absorption of solar radiation by clouds: observations versus models. Science 267: 496–499

CLIMAP Project Members (1976) The surface of the ice-age Earth. Science 191: 1131–1137

CLIMAP Project Members (1984) The last interglacial ocean. Quat Res 21: 123–224

Emanuel KA, Neelin JD, Bretherton CS (1994) On large-scale circulations in convecting atmospheres. Q J R Meteorol Soc 120: 1111–1143

Fu R, Liu WT, Dickinson EE (1996) Response of tropical clouds to the interannual variation of sea-surface temperature. J Clim 9: 616–634

Fu R, Del Genio AD, Rossow WB, Liu WT (1992) Cirrus-cloud thermostat for tropical sea surface temperatures tested using satellite data. Nature 358: 394–397

Ghil M, Childress S (1987) Topics in geophysical fluid dynamics: atmospheric dynamics, dynamo theory and climate dynamics. Springer, Berlin Heidelberg New York, pp 485

Goody RM, Yung YL (1989) Atmospheric radiation, 2nd edn. Oxford University Press, Oxford, UK, pp 519

Hartman DL, Ramanathan V, Berroir A, Hunt GE (1986) Earth radiation budget data and climate. Rev Geophys 24: 439–468

Hu Q, Randall DA (1994) Low frequency oscillations in radiative-convective systems. J Atmos Sci 51: 1089–1099

Ingersoll AP (1969) The runaway greenhouse. A history of water on Venus. J Atmos Sci 26: 1191–1198

James IN (1994) Introduction to circulating atmospheres. Cambridge University Press, Cambridge, UK, pp 422

Johnson RH, Ciesielski PE (2000) Rainfall and radiative heating rates from TOGA COARE atmospheric budgets. J Atmos Sci 57: 1497–1514

Kato S, Ackerman TP, Clothiaux EE, Mather JH, Mace GG, Wesely ML, Murcray F, Michalsky J (1997) Uncertainties in modeled and measured clear-sky surface shortwave irradiances. J Geophys Res 102 D22: 25 881–25 898

Komabayasi M (1967) Discrete equilibrium temperatures of a hypothetical planet with the atmosphere and the hydrosphere of one component-two phase system under constant solar radiation. J Meteorol Soc Japan 45: 137–138

Lau KM, Sui CH, Chou MD, Tao WK (1994) An enquiry into the cirrus-cloud thermostat effect for tropical sea-surface temperature. Geophys Res Lett 21: 1157–1160

Li ZX, Ide K, Le Treut H, Ghil M (1997) Atmospheric radiative equilibria in a simple column model. Clim Dyn 13: 429–440

Liou KN (1992) Radiation and cloud processes in the atmosphere: theory, observation and modeling. Oxford University Press, Oxford, UK, pp 487

Madden R, Julian PR (1971) Detection of a 40–50 day oscillation in the zonal wind in the tropical Pacific. J Atmos Sci 28: 1109–1123

Manabe S, Wetherald RT (1967) Thermal equilibrium of the atmosphere with a given distribution of relative humidity. J Atmos Sci 24: 241–259

Morcrette JJ (1991) Radiation and cloud radiative properties in the European Center for Medium-Range Weather Forecasts forecasting system. J Geophys Res 96D: 9121–9132

Nakajima S, Hayashi YY, Abe Y (1992) A study of the "runaway greenhouse effect" with a one-dimensional radiative-convective model. J Atmos Sci 49: 2256–2266

Neelin JD, Yu JY (1994) Modes of tropical variability under convective adjustment and the Madden-Julian oscillation. Part I: analytical results. J Atmos Sci 51: 1876–1894

North GR, Cahalan RF, Coakley JA Jr (1981) Energy balance climate models. Rev Geophys Space Phys 19: 91–121

Peixoto JP, Oort AH (1992) Physics of climate. American Institute of Physics, New York, pp 520

Pierrehumbert RT (1995) Thermostats, radiator fins, and the local runaway greenhouse. J Atmos Sci 52: 1784–1806

Ramanathan V, Collins W (1991) Thermodynamic regulation of ocean warming by cirrus clouds deduced from observations of the 1987 El Niño Nature 351: 27–32

Ramanathan V, Collins W (1993) A thermostat in the tropics. Nature 361: 410–411

Rennó NO (1997) Multiple equilibria in radiative-convective atmospheres. Tellus 49A: 423–438

Simpson GC (1927) Some studies in terrestrial radiation. Mem R Meteorol Soc 2: 16

Shine KP, Sinha A (1991) Sensitivity of the Earth's climate to height-dependent changes in the water vapour mixing ratio. Nature 354: 382–384

Zeng N, Neelin JD (1999) A land-atmosphere interaction theory for the tropical deforestation problem. J Clim 12: 857–872